164

Copy No.
RM No. A7K28

NACA

RESEARCH MEMORANDUM

HIGH-SPEED STABILITY AND CONTROL CHARACTERISTICS

OF A FIGHTER AIRPLANE MODEL WITH A

SWEPT-BACK WING AND TAIL

By Charles P. Morrill, Jr. and Lee E. Boddy

Ames Aeronautical Laboratory
Moffett Field, Calif.

NATIONAL ADVISORY COMMITTEE
# FOR AERONAUTICS
WASHINGTON
April 14, 1948

NATIONAL ADVISORY COMMITTEE FOR AERONAUTICS

RESEARCH MEMORANDUM

HIGH-SPEED STABILITY AND CONTROL CHARACTERISTICS

OF A FIGHTER AIRPLANE MODEL WITH A

SWEPT-BACK WING AND TAIL

By Charles P. Morrill, Jr. and Lee E. Boddy

SUMMARY

The results of wind-tunnel tests conducted to determine the high-speed stability and control characteristics of an airplane model with a swept-back wing and tail are presented in this report. There are included the aerodynamic coefficients and the longitudinal- and lateral-control characteristics of the plain wing-fuselage-tail combination. Also included are the effects of wing leading-edge slats and fuselage-side dive brakes.

Divergence of the drag occurred at approximately 0.86 Mach number and was accompanied by an increase in static longitudinal stability. However, no uncontrollable tendency to pitch down at high speeds was noted. The leading-edge slats proved effective in delaying the stall and instability at high lift coefficients but caused longitudinal instability at low lift coefficients and high Mach numbers. Each 10° deflection of the dive brakes increased the drag coefficient approximately 0.007 and increased the pitching-moment coefficient about the same amount as a 0.7° upward elevator deflection.

INTRODUCTION

This report presents the high-speed stability and control characteristics of a fighter airplane model with a 35° swept-back wing and tail. The data presented herein were obtained from tests made in the Ames 16-foot high-speed wind tunnel of a semispan model of the airplane. For results of other tests conducted with the same model, consult references 1 and 2 which cover modifications to the original model and the effects of external stores, respectively.

The high-speed data contained in this report included the basic aerodynamic characteristics of the model, the effectiveness and hinge-moment characteristics of the control surfaces, the effect of wing leading-edge slats, and the effect of the fuselage-side dive brakes.

SYMBOLS

The symbols used in this report are defined as follows:

R Reynolds number

M Mach number

α angle of attack of fuselage reference line, degrees

C_L lift coefficient $\left(\dfrac{\text{twice lift of half model}}{qS}\right)$

C_D drag coefficient $\left(\dfrac{\text{twice drag of half model}}{qS}\right)$

C_m pitching-moment coefficient $\left(\dfrac{\text{twice pitching moment of half model}}{qS\ \text{M.A.C.}}\right)$

δ_e elevator deflection about hinge line, degrees

i_t stabilizer incidence relative to fuselage reference line, degrees

C_{h_e} elevator hinge-moment coefficient
$$\left(\frac{\text{twice elevator hinge moment of half model}}{q\ b_e\ \overline{c_e^2}}\right)$$

C_{h_t} stabilizer hinge-moment coefficient
$$\left(\frac{\text{twice stabilizer hinge moment of half model}}{q\ S_t\ \text{M.A.C.}_t}\right)$$

F_s stick force, pounds $\left(C_{h_e}\ q\ b_e\ \overline{c_e^2}\times\dfrac{\delta_e}{\delta_s l_s}\right)$

C_l rolling-moment coefficient $\left(\dfrac{\text{rolling moment of half model}}{qSb}\right)$

δ_a aileron deflection about hinge line, degrees

C_{h_a} aileron hinge-moment coefficient $\left(\dfrac{\text{aileron hinge moment}}{q \, b_a \, \overline{c_a^2}} \right)$

δ_B fuselage-side dive-brake inner-door deflection, degrees

where

q free-stream dynamic pressure, pounds per square foot

S twice wing area of half model, square feet

M.A.C.   mean aerodynamic chord of wing, feet

b twice the wing semispan, feet

b_e twice elevator hinge-line length, feet

$\overline{c_e^2}$ mean square chord of elevator normal to hinge line, square feet

S_t twice horizontal tail area of half model, square feet

M.A.C.$_t$ mean aerodynamic chord of horizontal tail, feet

δ_s stick deflection, degrees

l_s stick length, feet

b_a aileron hinge-line length, feet

$\overline{c_a^2}$ mean square chord of aileron normal to hinge line, square feet

MODEL AND APPARATUS

A semispan, 0.20-scale model of a fighter airplane with 35° swept-back wing and tail was employed in these tests, which were conducted in the Ames 16-foot high-speed wind tunnel. The half model was mounted on the trunnion of the wind-tunnel balance frame with its center plane approximately 6 inches from the tunnel wall as shown in figure 1. A steel separation plate fastened to the turntable in the tunnel wall by means of a fairing served as a reflection plane for the half model. (See reference 1 for sketch and more detailed description of the installation.)

The model was tested without canopy, dorsal fin, or vertical tail. The horizontal tail was not equipped with trim tabs but the stabilizer was designed for variable incidence.

The wing of the model had a leading-edge slat of constant chord (24 percent of wing chord at the outboard end and 15 percent at the inboard end measured parallel to the center line) as shown in figure 2. The inboard end of the slat was 10.82 inches from the fuselage center line. The span of the slat was 31.05 inches (69 percent of the wing semispan) measured normal to the center line; and the chord was 3.29 inches measured parallel to the center line. Brackets of various lengths were used to fasten the slat to the wing in the closed, one-quarter extended, one-half extended, or fully extended position. The maximum extension was 1.461 inches normal to the wing leading edge, the chordwise extension then being 10.7 percent at the outboard end and 6.7 percent at the inboard end measured parallel to the center line. The maximum extension was accompanied by a tilt or droop of the slat 9° 36' below the wing reference plane. For intermediate extensions the droop was proportionally smaller.

A dive brake of the folding-door type was incorporated in the side of the fuselage. (See fig. 3.) The inner door pivoted about a hinge line at fuselage station 65.2. The combined area of both doors of the brake was 0.298 square feet (4.3 percent of the wing area of the half model) and the chord of the inner door was 0.471 feet. In addition to the normally closed position the dive brake could be deflected 20°, 40°, or 85°, the angle being measured between the inner door and its closed position.

Pertinent model dimensions are:

Wing

Area (whole model), sq ft 11.516

Span (whole model), ft 7.423

Aspect ratio 4.785

Taper ratio 0.513

Dihedral, deg 3.0

Mean aerodynamic chord, ft 1.617

Sweepback of 25-percent-chord line, deg 35.22

Root incidence, deg 1.0

Tip incidence, deg . . . .   -1.0

Root airfoil section[1] . . . . modified NACA 0012–64

Tip airfoil section[1] . . . . modified NACA 0011–64

Aileron (one only)

Area (aft of hinge line), sq ft 0.746

Span, ft 2.008

Mean square chord, sq ft 0.154

Horizontal Tail

Area (whole model), sq ft 1.400

Span (whole model) ft 2.550

Aspect ratio 4.650

Taper ratio 0.450

Dihedral, deg 10.0

Mean aerodynamic chord, ft 0.578

Sweepback of 25–percent–chord line, deg 35.59

Airfoil section (parallel to
   center line) . . . . NACA 0010–64

Elevator

Area (whole model), sq ft 0.405

Span (whole model), ft 2.310

Mean square chord, sq ft 0.0248

Stabilizer

Area (whole model), sq ft 0.995

Span (whole model), ft 2.550

---

[1]Both sections taken normal to 25–percent–chord line. (See reference
1 for details on modification to section.)

TESTS

The investigation consisted of a determination of the general characteristics of the half model and a study of the effects of the wing leading—edge slats and the fuselage dive brakes on these characteristics. As indicated in the definitions of symbols, the data have been modified to apply to a whole model and the discussion following will be on the basis of a complete model.

The slats were tested in the closed, one—quarter extended, one—half extended, and fully extended positions. Data were obtained for dive brake deflections of 0°, 20°, 40°, and 85°.

The test Reynolds number, based on the mean aerodynamic chord of the wing, varied from 3.35 million at 0.30 Mach number to 6.20 million at a Mach number of 0.90. (See fig. 4.)

Pitching moments are referred to a center 2.68 inches above the 25—percent point of the mean aerodynamic chord of the wing (fuselage station 37.70). The horizontal—tail hinge moments are given about a hinge axis 1.44 inches below the 4.3—percent point of the mean aerodynamic chord of the tail.

No tare corrections have been applied to the data since no part of the support system was exposed to the main air stream. The effects of the wind—tunnel walls on the angle of attack, drag, and pitching moment have not been accounted for since they are small for a model of this size and, in general, have the opposite effect of the leakage. Also, no correction has been applied to the aileron effectiveness to account for the end—plate effect of the reflection plane. The aileron effectiveness of the half model agreed well with that obtained from preliminary tests of the whole model mounted in the center of the wind tunnel. However, constriction effects of the model and support system have been taken into account. Since the model was small relative to the test section the constriction correction to the Mach number was less than 2 percent at 0.90 Mach number.

The magnitude of the drag coefficients appears to be too large due to the effects of leakage air passing over the supporting structure inside the fairing. However, the variation of drag with Mach number is believed to be reliable.

RESULTS AND DISCUSSION

Figure 4 gives the average variation of Reynolds number with Mach number during the tests. The basic characteristics of the model are presented in figures 5 through 8. Longitudinal and lateral

characteristics for zero yaw together with accompanying control-surface hinge moments are given in figures 9 through 16. Figures 17 to 21 present the effect of the wing slats; and data on the dive brake are given in figures 22 through 25.

Lift, Drag, and Pitching Moment

The variation of lift coefficient with angle of attack and Mach number is presented in figure 5. The average slope of the lift curve increased with increasing Mach number, but the angle of attack for zero lift remained essentially constant up to 0.90 Mach number.

At low lift coefficients the drag coefficients remained relatively constant to a Mach number of about 0.86, at which divergence occurred. At higher lift coefficients the divergence Mach number was lowered to approximately 0.825. (See fig. 6.)

The variation of pitching-moment coefficient with lift coefficient of the model with the horizontal tail removed indicated longitudinal instability at Mach numbers up to approximately 0.85, at which the model became neutrally stable. (See fig. 7.) At higher Mach numbers the model exhibited stable characteristics. The pitching-moment coefficient at zero lift showed only slight variation within the limits of the test (-0.008 to 0.003). Pitching-moment characteristics of the model with the horizontal tail (fig. 8) indicated static longitudinal stability for moderate lift coefficients at all test Mach numbers. However, a strong tendency existed for the model to become longitudinally unstable at the higher lift coefficients, especially with a negative deflection of the elevator or stabilizer.

Longitudinal Characteristics

Figure 9 presents the variation of lift- and pitching-moment-curve slopes with Mach number. At low lift coefficients the lift-curve slope increased gradually with Mach number. The curve for 0.4 lift coefficient shows a decrease of slope from low to medium Mach numbers followed by a gradual increase, reaching a peak at 0.85 Mach number and decreasing rapidly thereafter.

The static instability exhibited below 0.85 Mach number by the model without the horizontal tail increased considerably at lift coefficients greater than 0.4. However, adding the tail restored stability for moderate lift coefficients at all Mach numbers within

the test limits. At lift coefficients above about 0.4 the degree
of stability was appreciably reduced. At a Mach number of 0.85
the longitudinal stability at zero lift began to increase; however,
the actual magnitude of the stability derivative did not exceed
controllable limits up to a Mach number of 0.90.

The approximate variation of elevator and stabilizer effective-
ness with Mach number is shown in figure 10. Inconsistencies in
the data prevented more detailed and accurate evaluation of these
parameters. However, the curves presented are believed to be
representative of the characteristics of these control surfaces.

The slope of the elevator—hinge—moment curves (fig. 11)
increased with Mach number for large elevator deflections but
decreased for small deflections. At small deflections there was
a tendency toward overbalance which actually occurred at a Mach
number of 0.875 with zero stabilizer incidence and an angle of
attack of 4°. While data for 4° angle of attack at 0.90 Mach
number are not available, indications are that overbalance would
have occurred. Little change in elevator hinge—moment coefficient
with change in stabilizer incidence was noticeable below about
0.85 Mach number.

Figure 12 presents the variation of stabilizer hinge—moment
coefficient with elevator deflection. The variations of hinge—moment
coefficient with both angle of attack and Mach number were relatively
constant within the range of the test. The variation of stabilizer
hinge—moment coefficient with stabilizer incidence is shown in figure 13.

The elevator angles required for level flight were calculated
with an assumed gross weight of 13,100 pounds. These deflections
together with the stick forces required to maintain balance at
several altitudes and zero stabilizer incidence are shown in figure
14. Since the stabilizer effectiveness was approximately 2 to 3
times that of the elevator, it is apparent that the stabilizer was
sufficiently effective to trim the model at all speeds included in
the range of the test.

Lateral Characteristics

As indicated by figure 15, the aileron effectiveness remained
essentially constant between Mach numbers of 0.3 and 0.90, although
there was some indication of reduced effectiveness at the higher
angles of attack at a Mach number of 0.90. At all other Mach numbers
within the range of the tests the effect of increasing the angle of

attack was noticeable but not serious. Figure 16 presents the
aileron hinge-moment coefficients.

Wing Leading-Edge Slats

The lift characteristics of the model for several positions
of the leading-edge slat are shown in figure 17. The effect of
delaying the stall at high lift coefficients is clearly apparent
at low Mach numbers. At a Mach number of 0.30 the extended slats
increased the lift coefficient at which stall occurred about 0.25.
At small angles of attack the extended slats reduced the lift
coefficient slightly. However, this effect is diminished as the
angle of attack is increased and is reversed at high angles.

At low lift coefficients the extended slats also caused an
increase in the drag coefficient of about 0.015 to 0.020. However,
because the extended slats delayed the stall, the drag coefficients
at high lift coefficients were smaller with the slats extended. The
increment of drag caused by the extended slats at low lift coeffi-
cients remained essentially constant with Mach number. (See fig. 18.)

Figures 19 and 20 show the effect of the slats on the pitching-
moment characteristics of the model. At low Mach numbers, the fully
extended slat alleviated the tip stall encountered with the slat
retracted, so that at the maximum lift coefficient the model was
longitudinally stable. However, for a small range of lift coefficients
immediately below the stall the model exhibited a tendency for
instability even with the slat extended. Extension of the slats at
Mach numbers above 0.80 and lift coefficients below 0.20 resulted
in serious loss of static longitudinal stability.

Figure 21 presents the effect of the slats on the aileron
effectiveness. In general, the slats decreased the effectiveness
of the aileron for upward deflections and increased it for downward
deflections. The effect was small in both cases. There is some
indication that the intermediate positions of the slats caused
greater loss than the extended positions.

Fuselage-Side Dive Brakes

Extending the fuselage dive brakes produced negligible effect
on the lift of the model. (See fig. 22.)

The increase in drag coefficient due to the dive brakes amounted to about 0.007 for each 10^0 deflection of the brake and increased only slightly with Mach number. (See fig. 23.)

Figure 24 shows that the dive brakes supplied a positive pitching-moment increment to the model approximately equal in effect to 0.7^0 of elevator deflection for each 10^0 of brake deflection, giving a maximum effect comparable to about 6^0 of upward elevator deflection with the brake completely extended. No important effect on the static longitudinal stability was noted.

The effectiveness of the elevator was reduced approximately 35 percent with the dive brakes deflected 85^0, as indicated in figure 25. The percentage loss in effectiveness remained relatively constant with Mach number. (Discretion should be employed in the use of fig. 25 as the limited amount of data obtained was somewhat erratic.)

CONCLUSIONS

The following conclusions may be drawn from the preceding discussion:
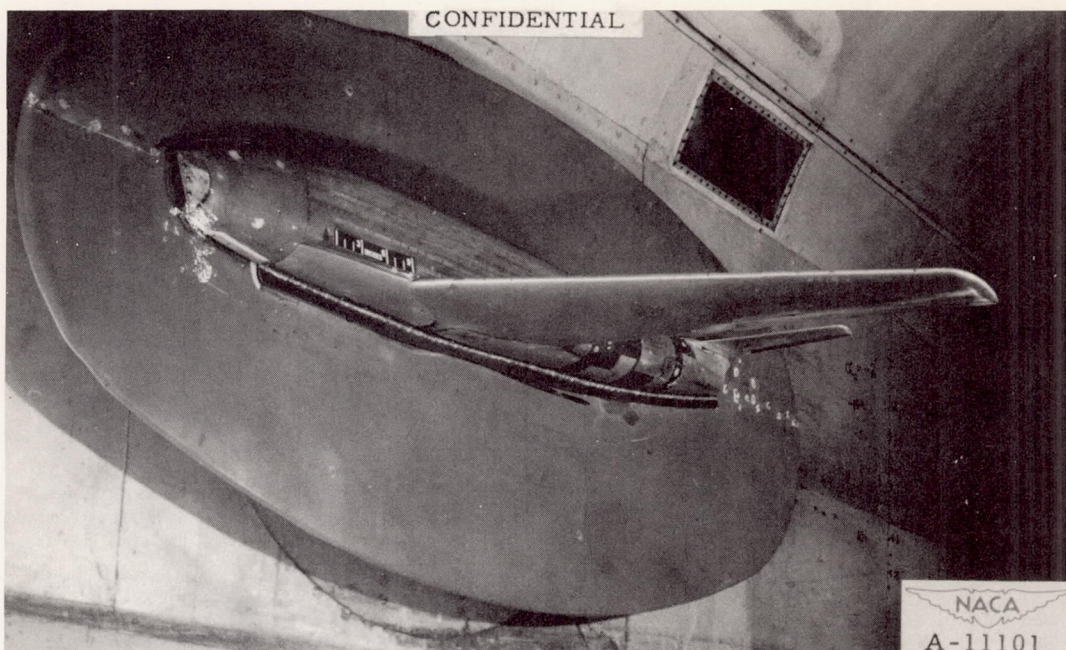
1. At low lift coefficients divergence of the drag occurred at a Mach number of approximately 0.86.

2. The model exhibited no uncontrollable tendency to nose down at Mach numbers within the limits of the tests (0.30 to 0.90).

3. Static longitudinal stability began to increase at a Mach number of about 0.85 but did not exceed controllable limits within the range of the tests.

4. The extended wing-leading-edge slats cause longitudinal instability at low lift coefficients and high Mach numbers but were otherwise effective in delaying the stall at high angles of attack and preventing instability at high lift coefficients.

5. Each 10^0 deflection of the fuselage-side dive brakes supplied a drag-coefficient increment of about 0.007 and an increment of positive pitching moment about equal that produced by 0.7^0 upward elevator deflection.

6. The effectiveness of the elevator was reduced about 35 °
percent with the dive brakes deflected 85°.
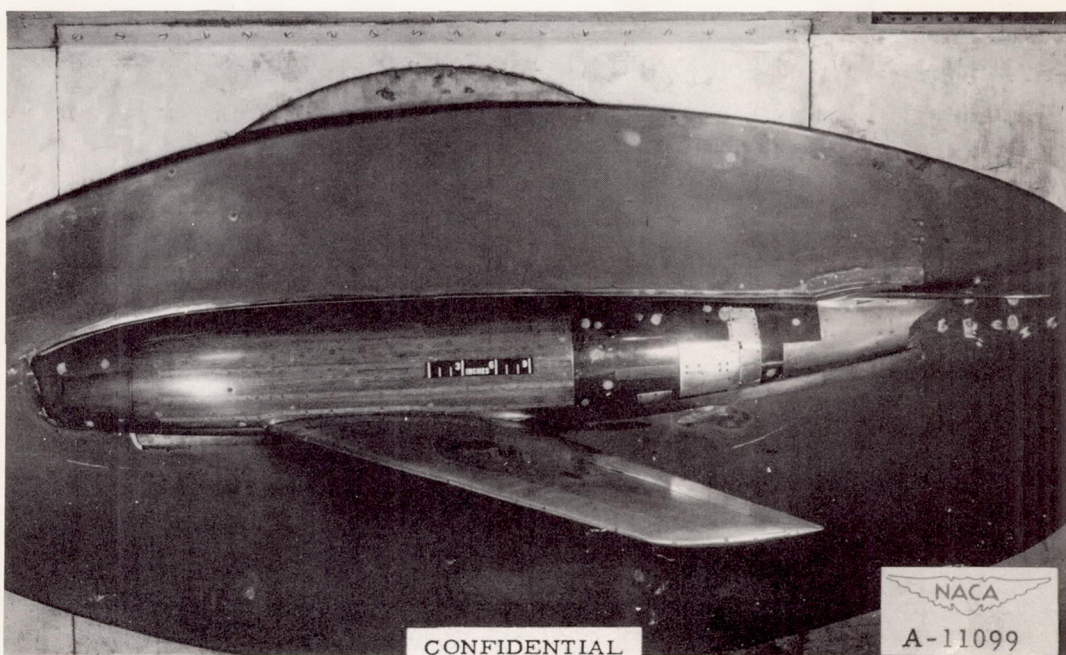
Ames Aeronautical Laboratory,
    National Advisory Committee for Aeronautics,
        Moffett Field, Calif.

REFERENCES

1. Boddy, Lee E., and Morrill, Charles P., Jr.: The Aerodynamic
    Effects of Modifications to the Wing and Wing-Fuselage
    Intersection of an Airplane Model with the Wing Swept Back
    35°. NACA CRM No. A7J02, 1947.

2. Boddy, Lee E., and Morrill, Charles P., Jr.: The Aerodynamic
    Effects of Rockets and Fuel Tanks Mounted Under the Swept-
    Back Wing of an Airplane Model. NACA CRM No. A7J03, 1947.
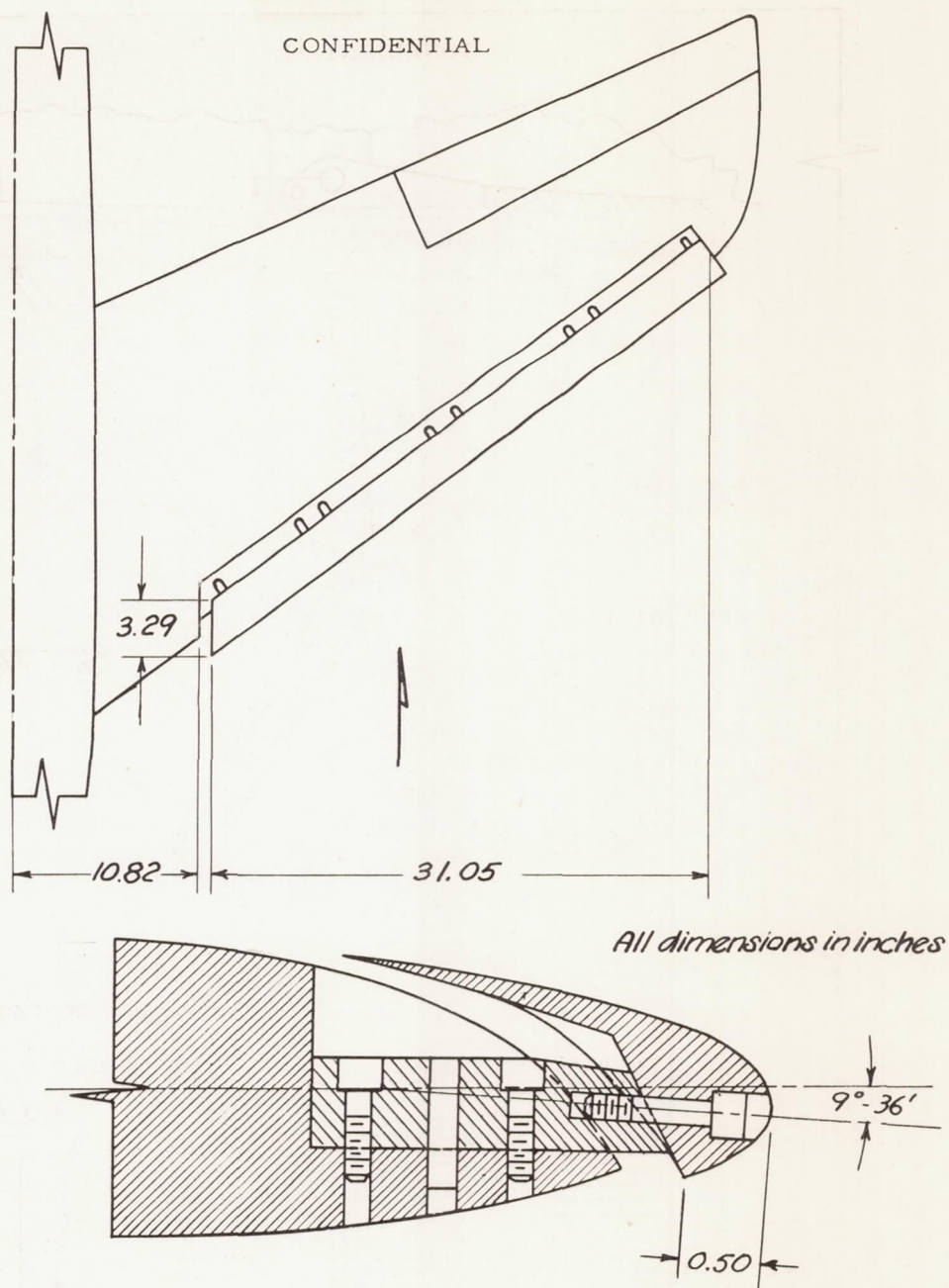
(a) Three-quarter front view.

(b) Side view.

Figure 1.— Semispan model mounted in wind tunnel.

CONFIDENTIAL

3.29

10.82

31.05

All dimensions in inches

9° - 36'

0.50

Typical section through slat and bracket

NACA
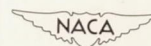
Figure 2.— Plan and detail of wing-leading-edge slat

CONFIDENTIAL

δ_B

5.651

3.438

8.208

Fus sta 81.2
.25 M.A.C._t

Fus sta 65.2

air flow

Fus sta 37.7
.25 M.A.C.

5.645

All dimensions in inches

Fus ref plane

Fus sta 0

1.99

.9

4.710

5.010

Front elevation of extended dive brake

NACA
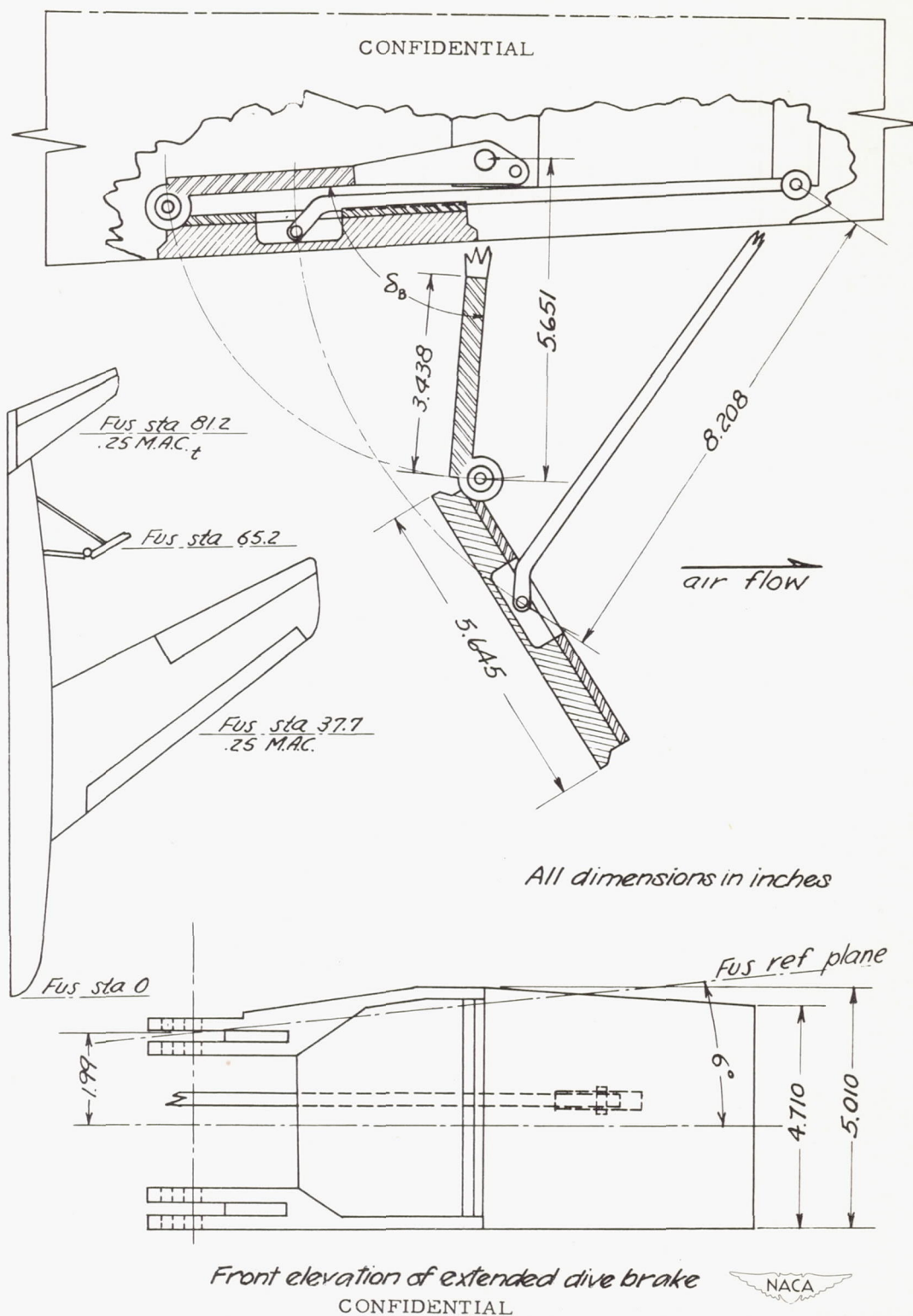
CONFIDENTIAL

Figure 3.- Plan and detail of fuselage-side dive brake
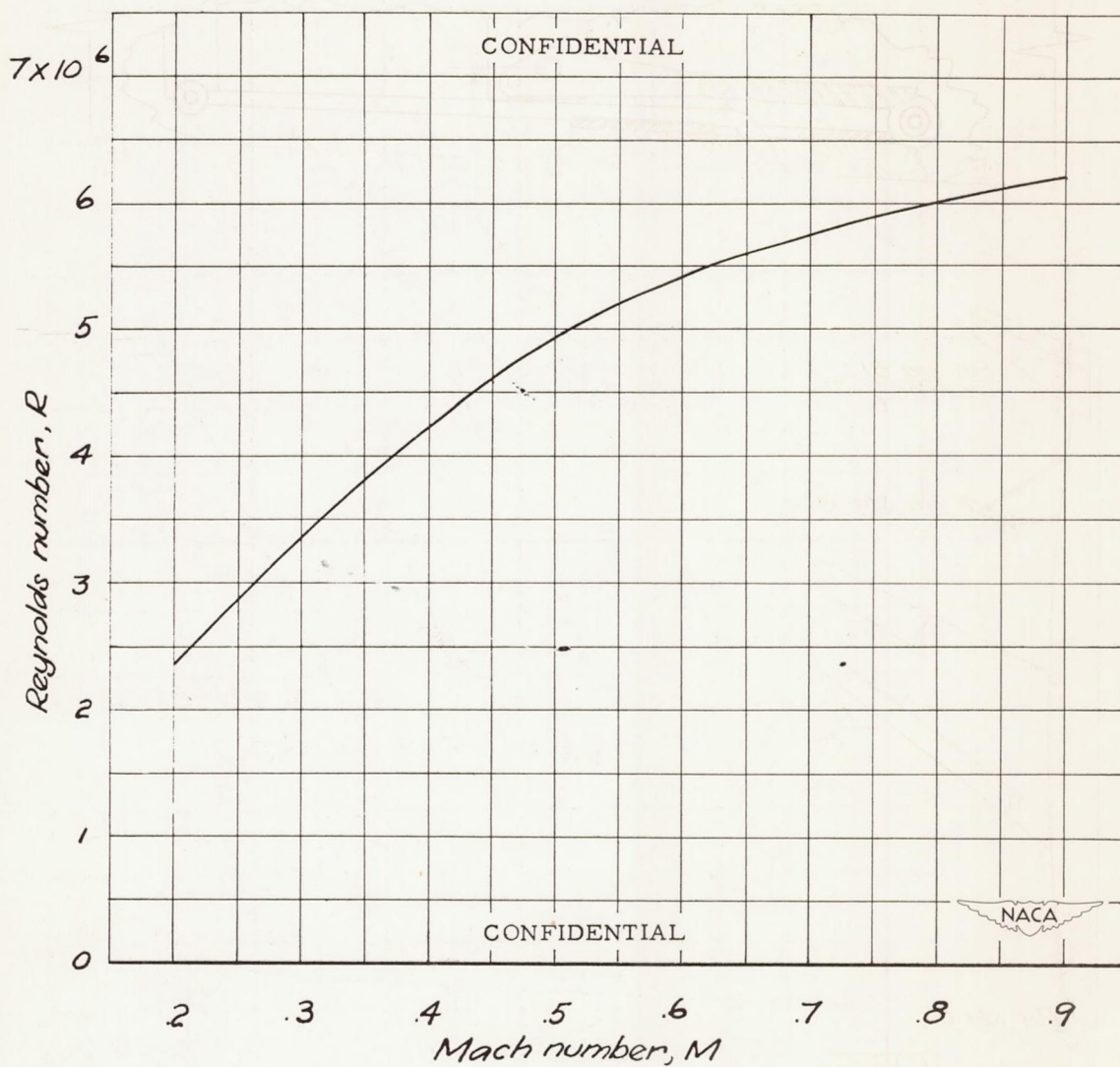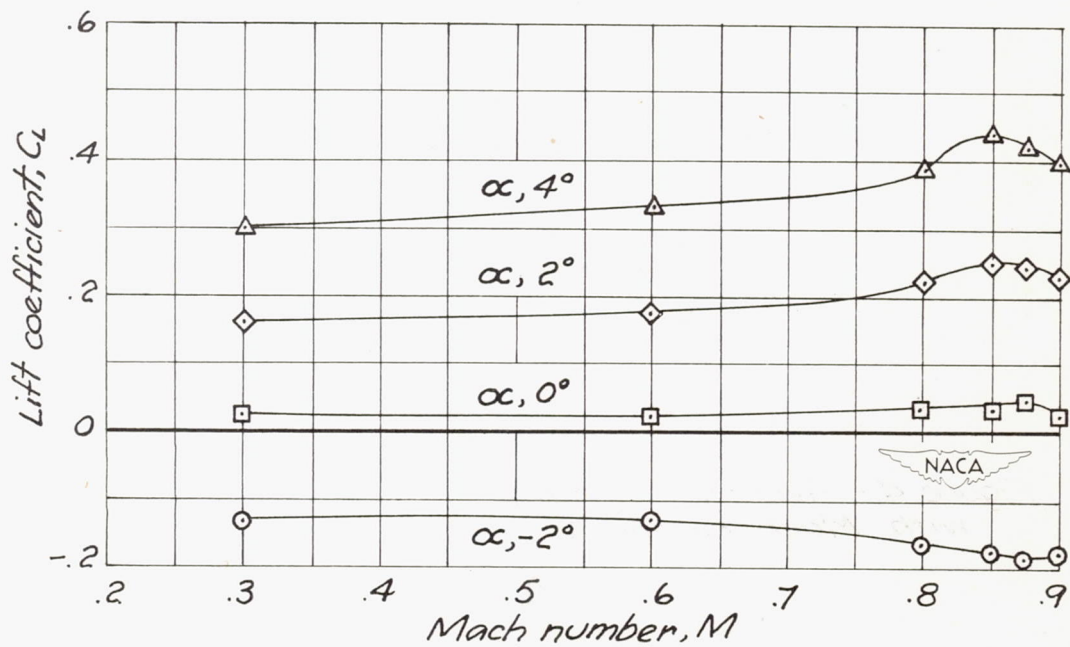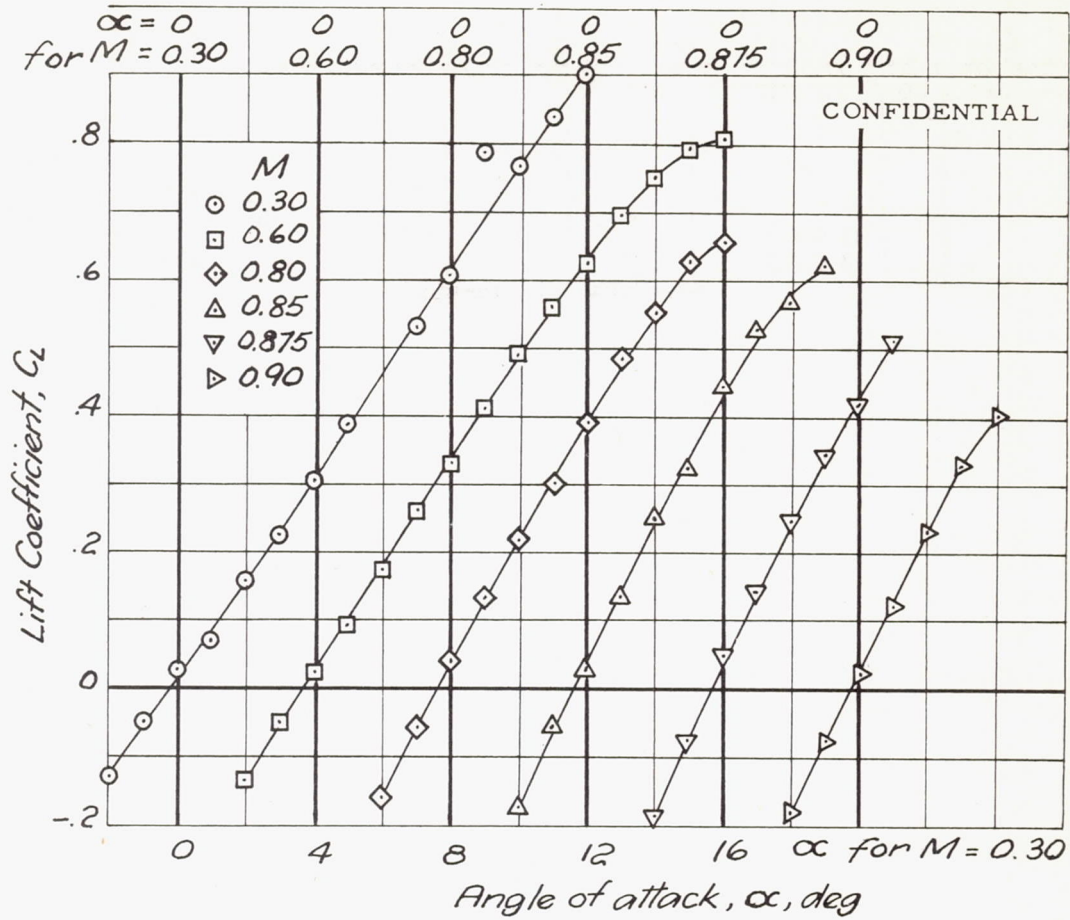
Figure 4.- Average variation of Reynolds number with Mach number

Figure 5.- Lift characteristics of the model
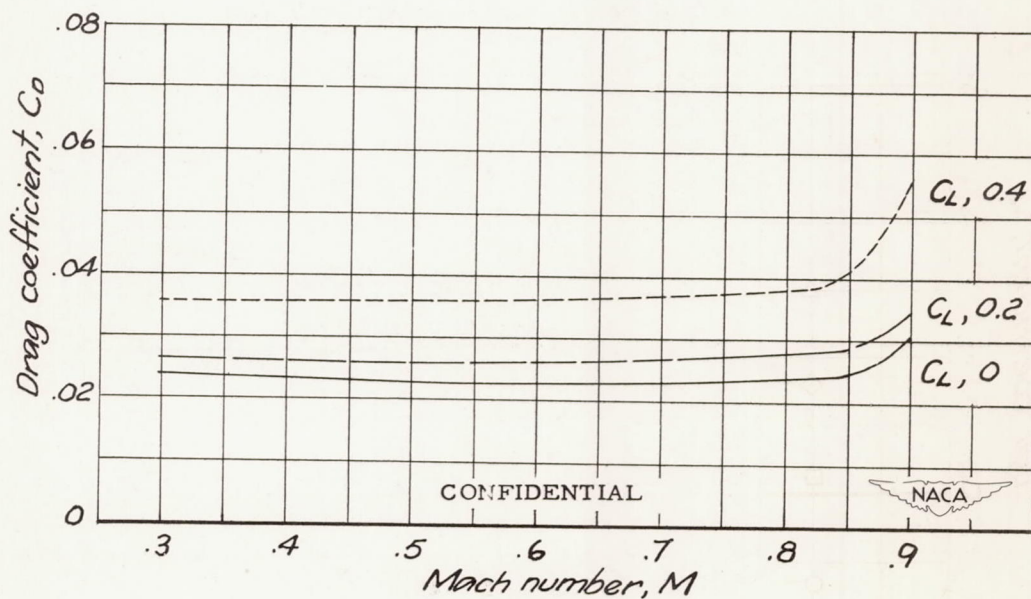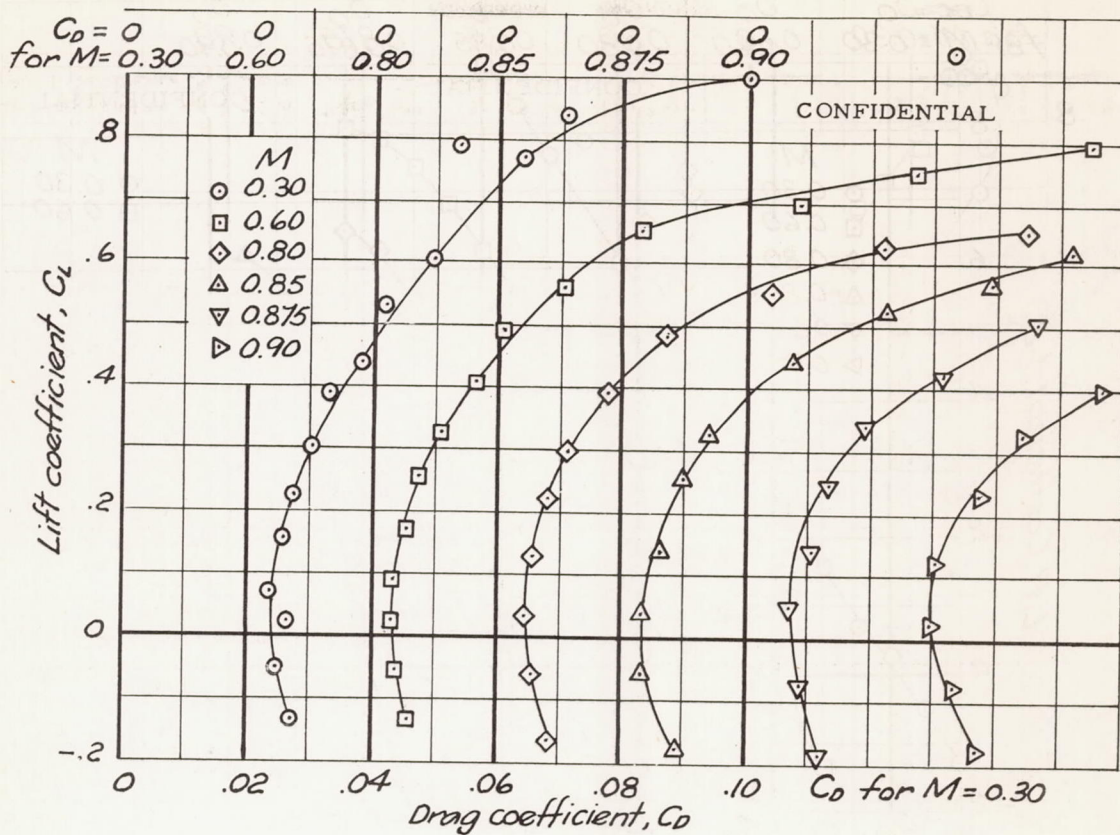
Figure 6. — Drag characteristics of the model
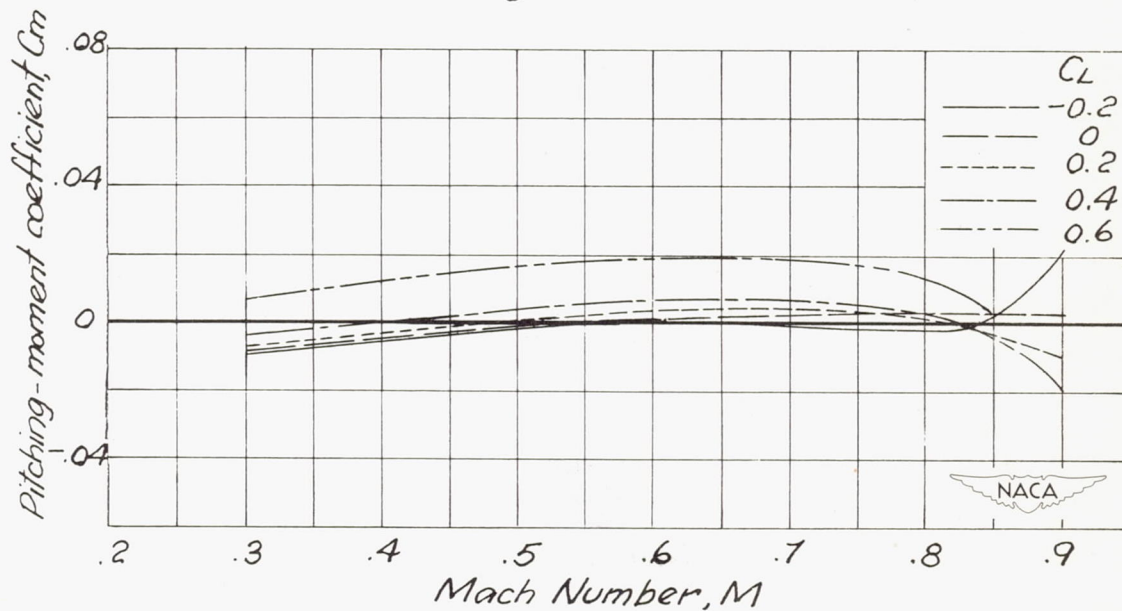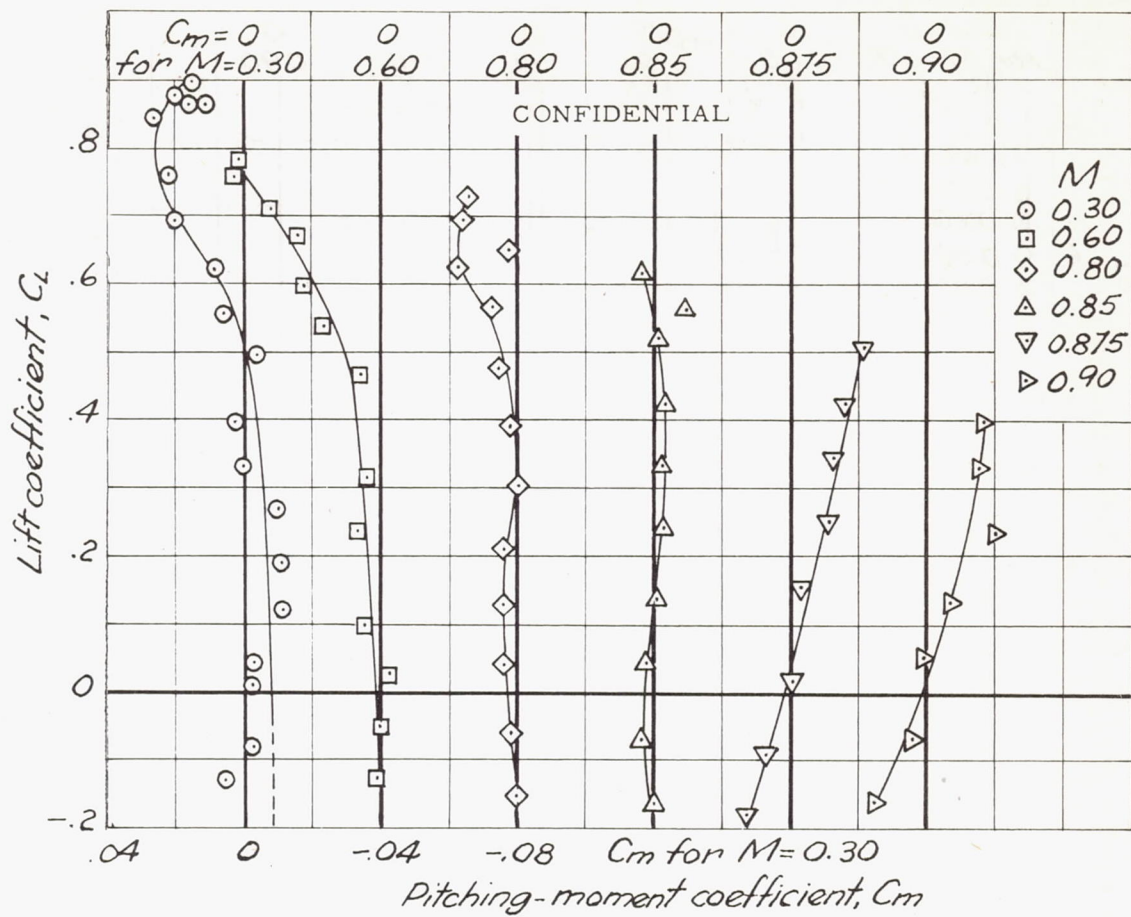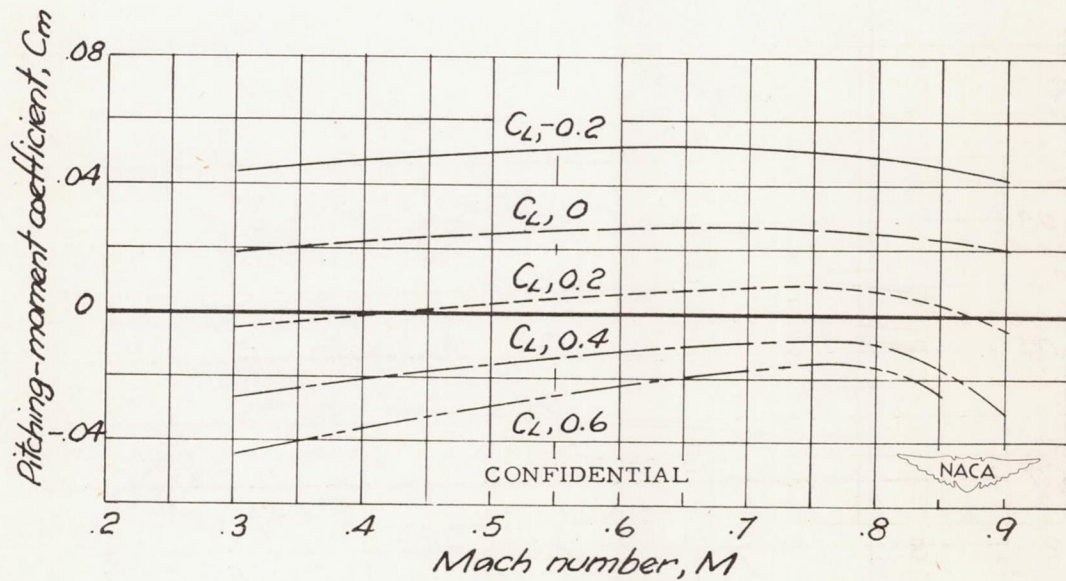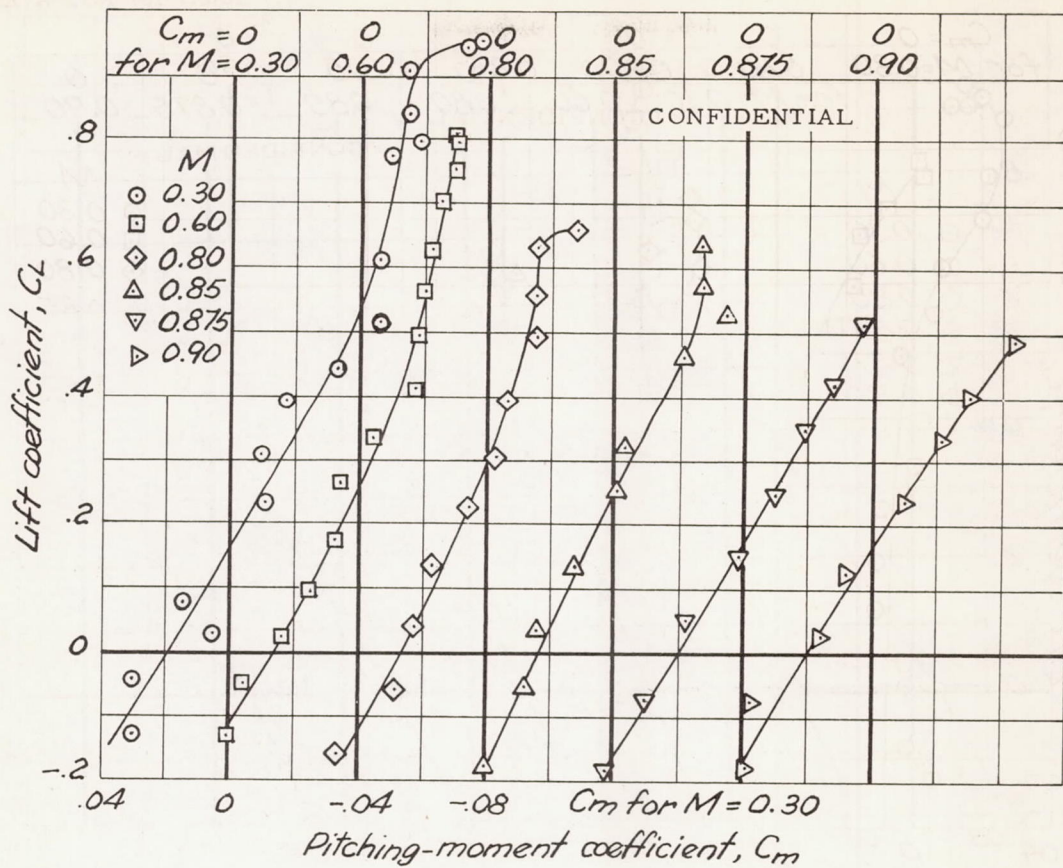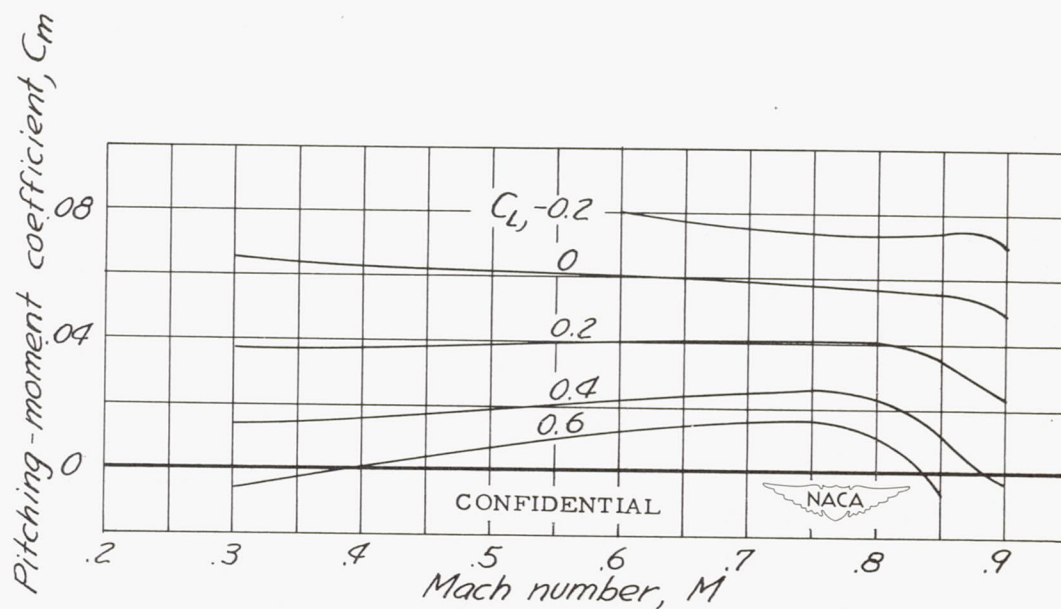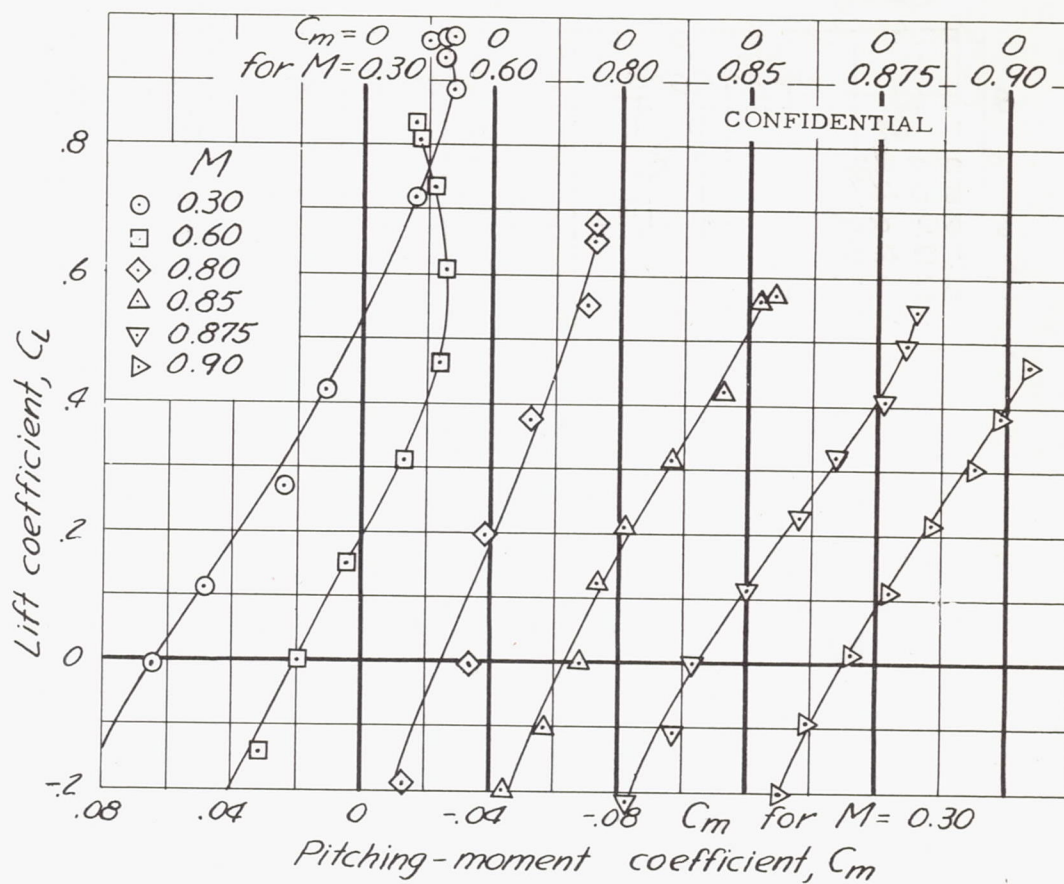
Figure 7.— Pitching-moment characteristics of the model without horizontal tail
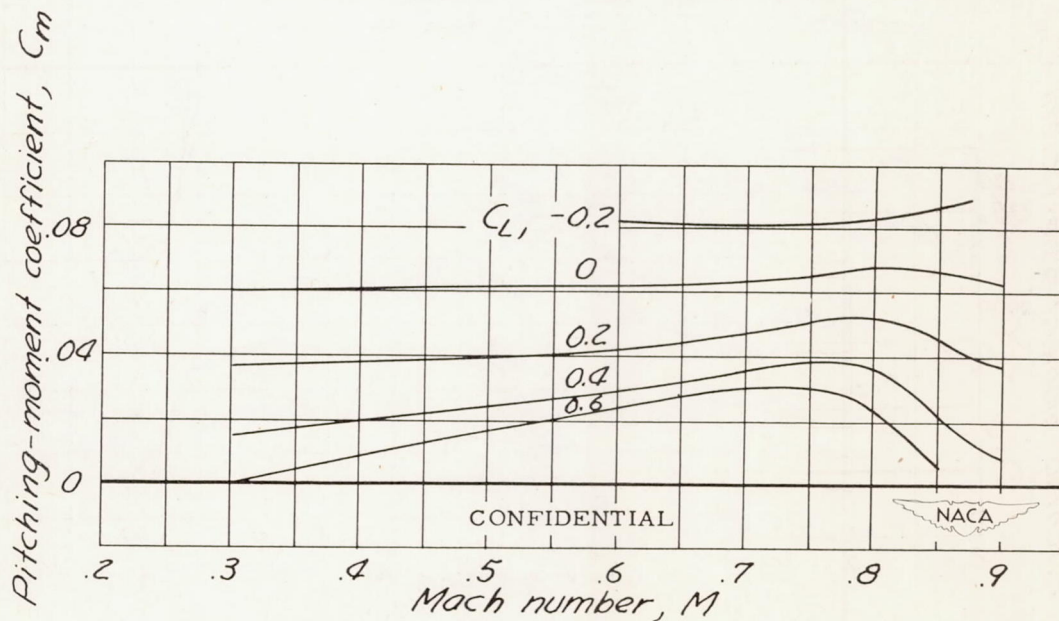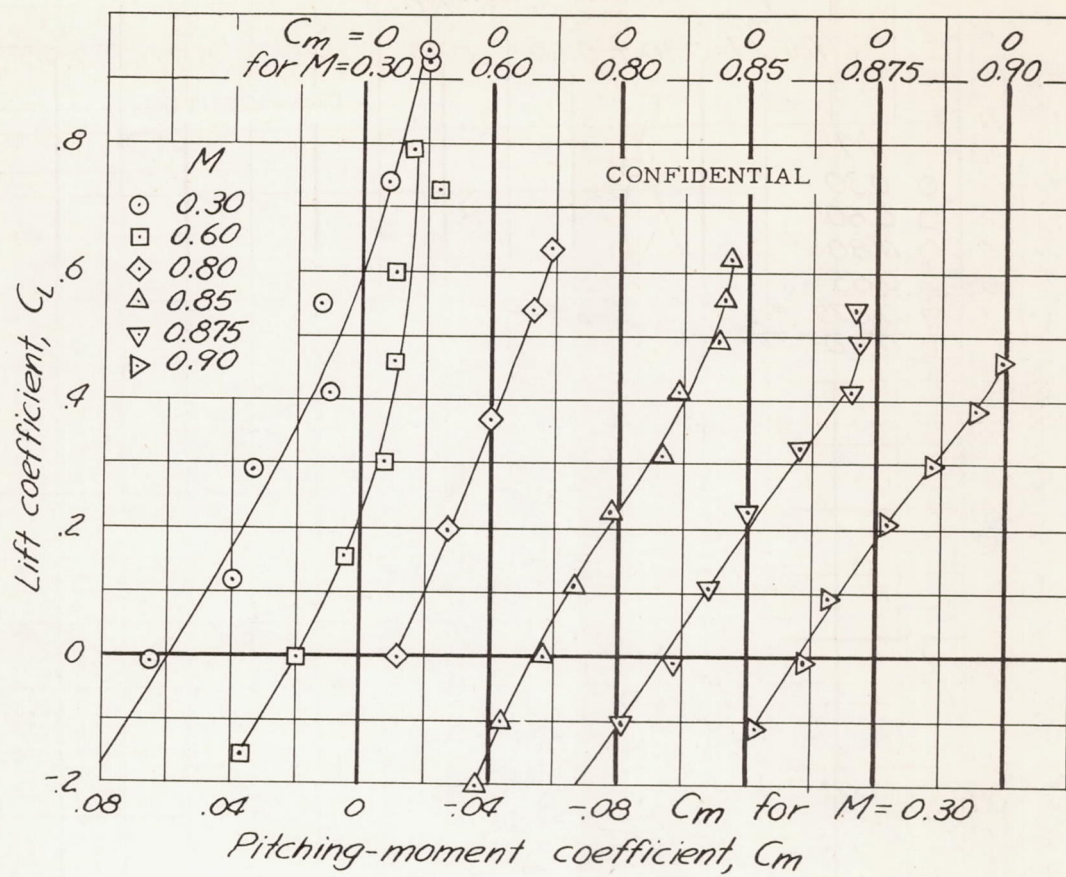
(a) Stabilizer and elevator neutral

Figure 8.- Pitching-moment characteristics of
the model with horizontal tail

(b) stabilizer neutral, elevator deflected -5°

Figure 8.-(Continued)

(c) Stabilizer deflected -3°, elevator neutral

Figure 8.- (Concluded)
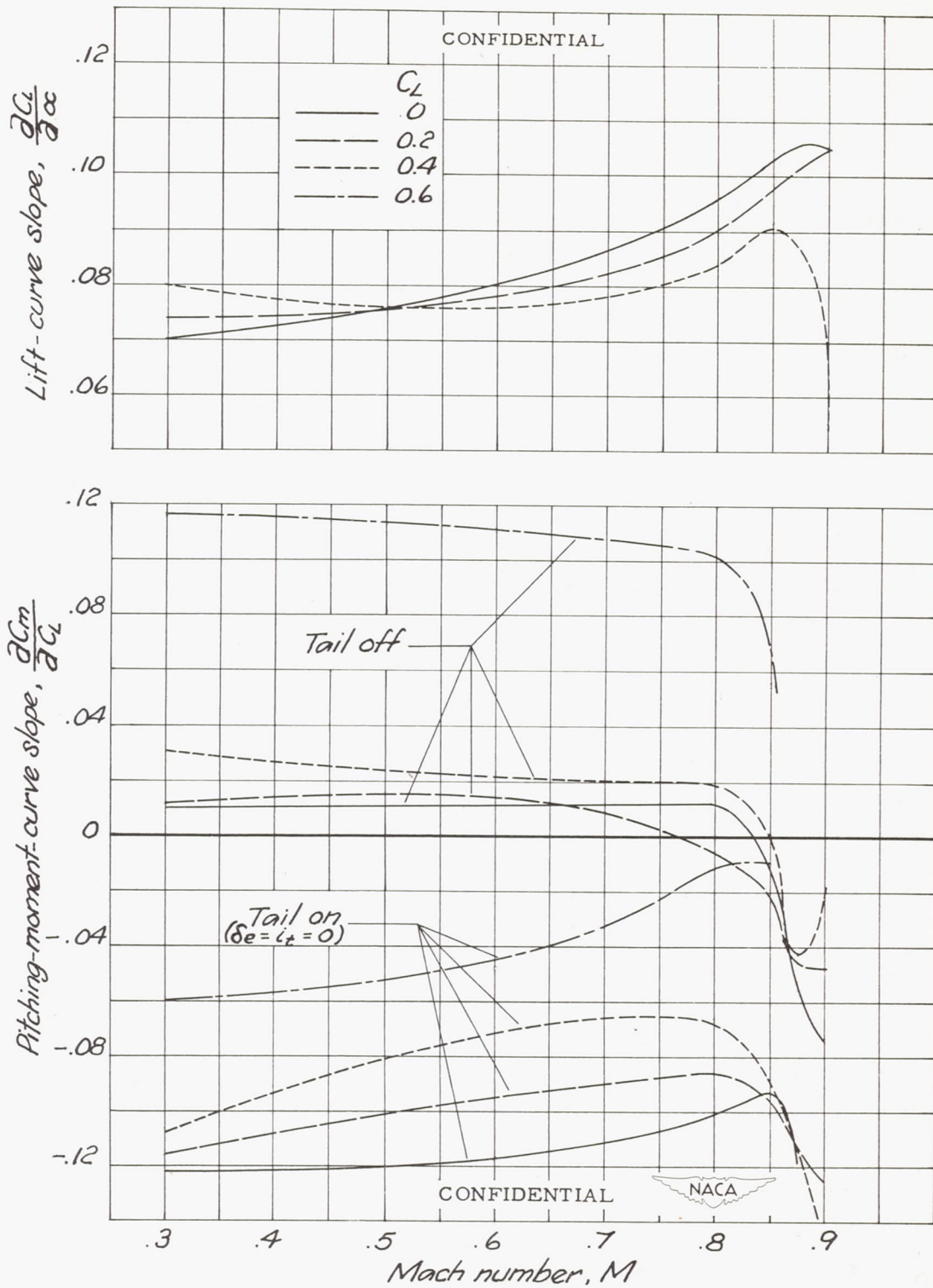
Figure 9.— Variation of lift-curve and pitching-
   moment-curve slopes with Mach number
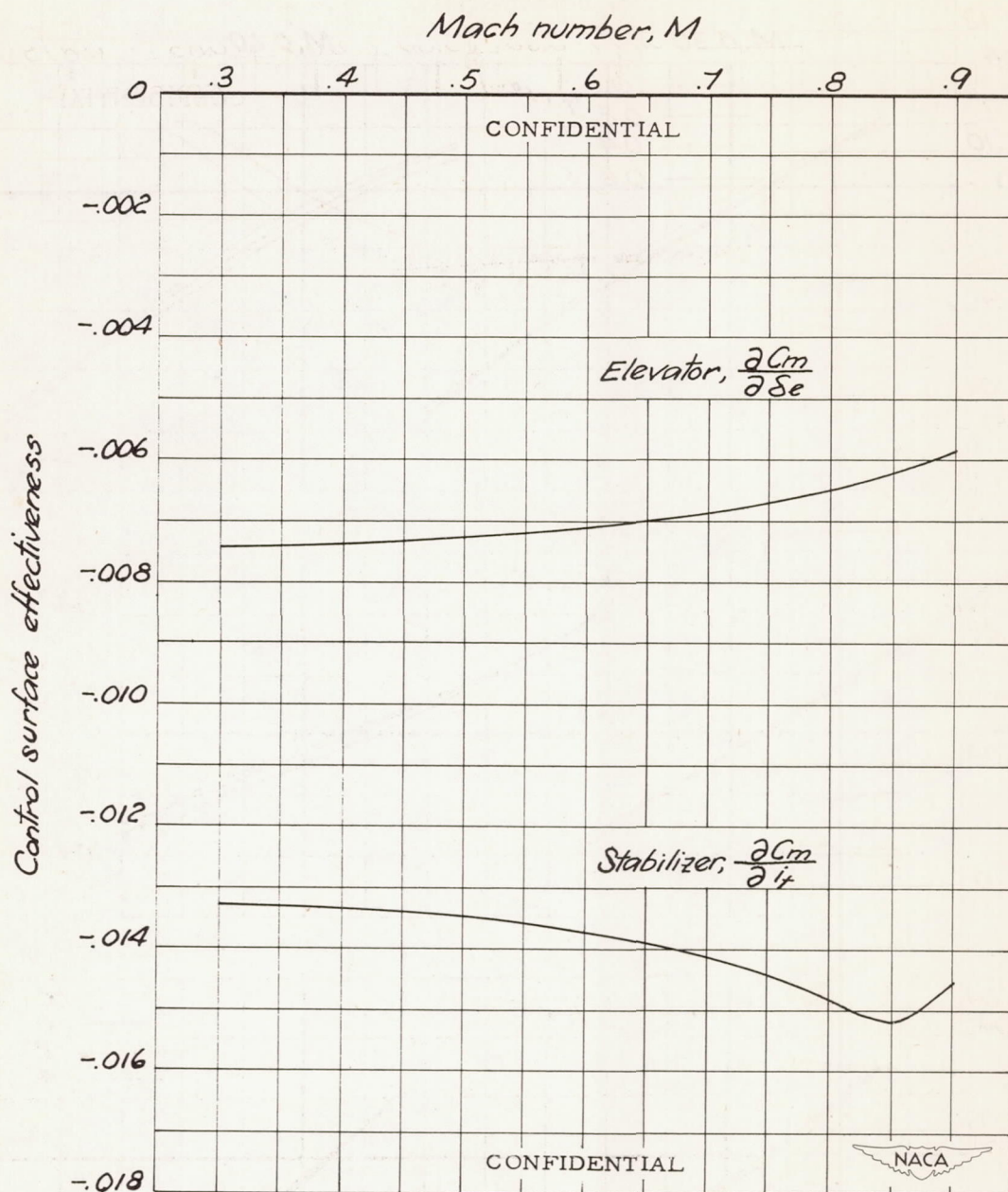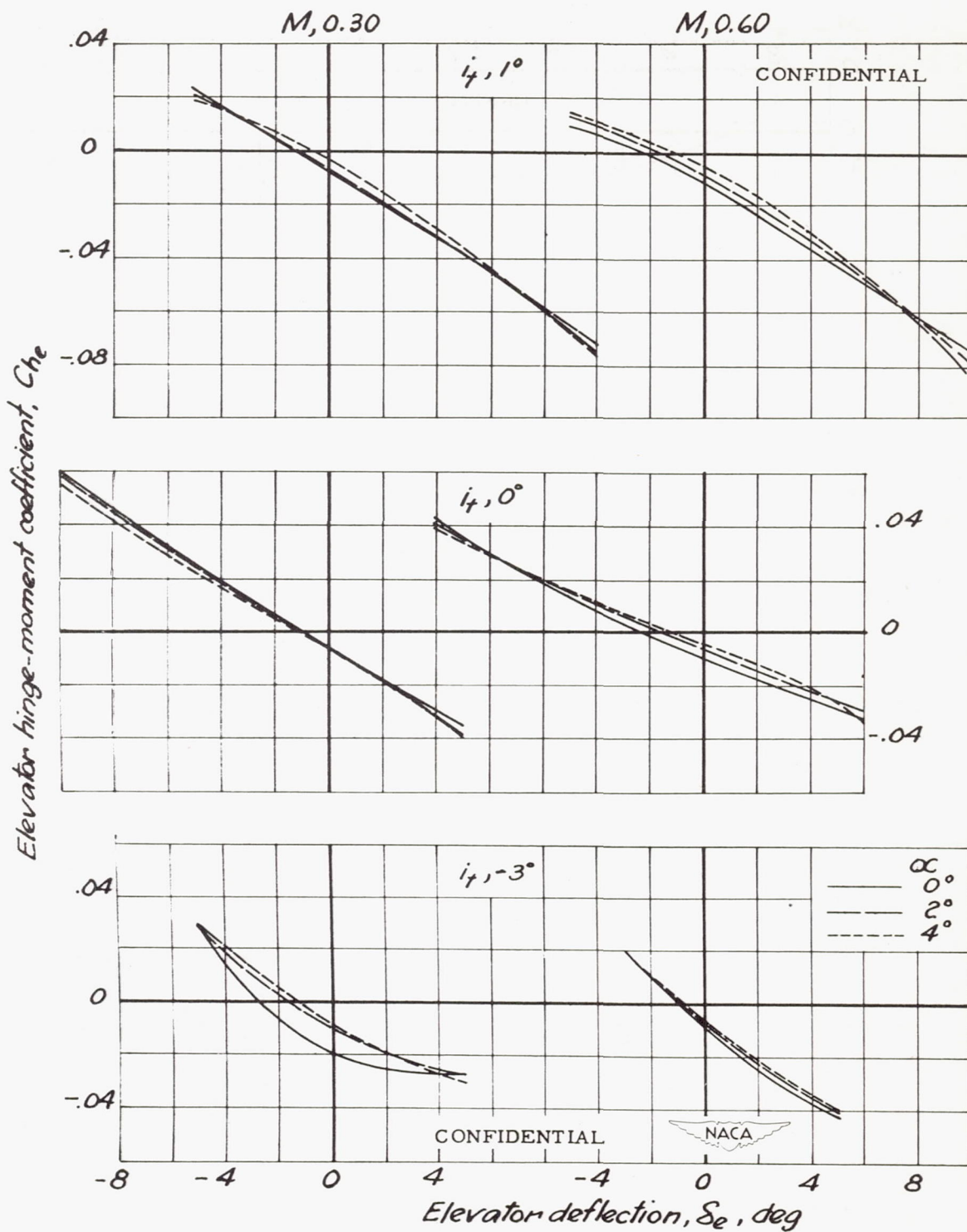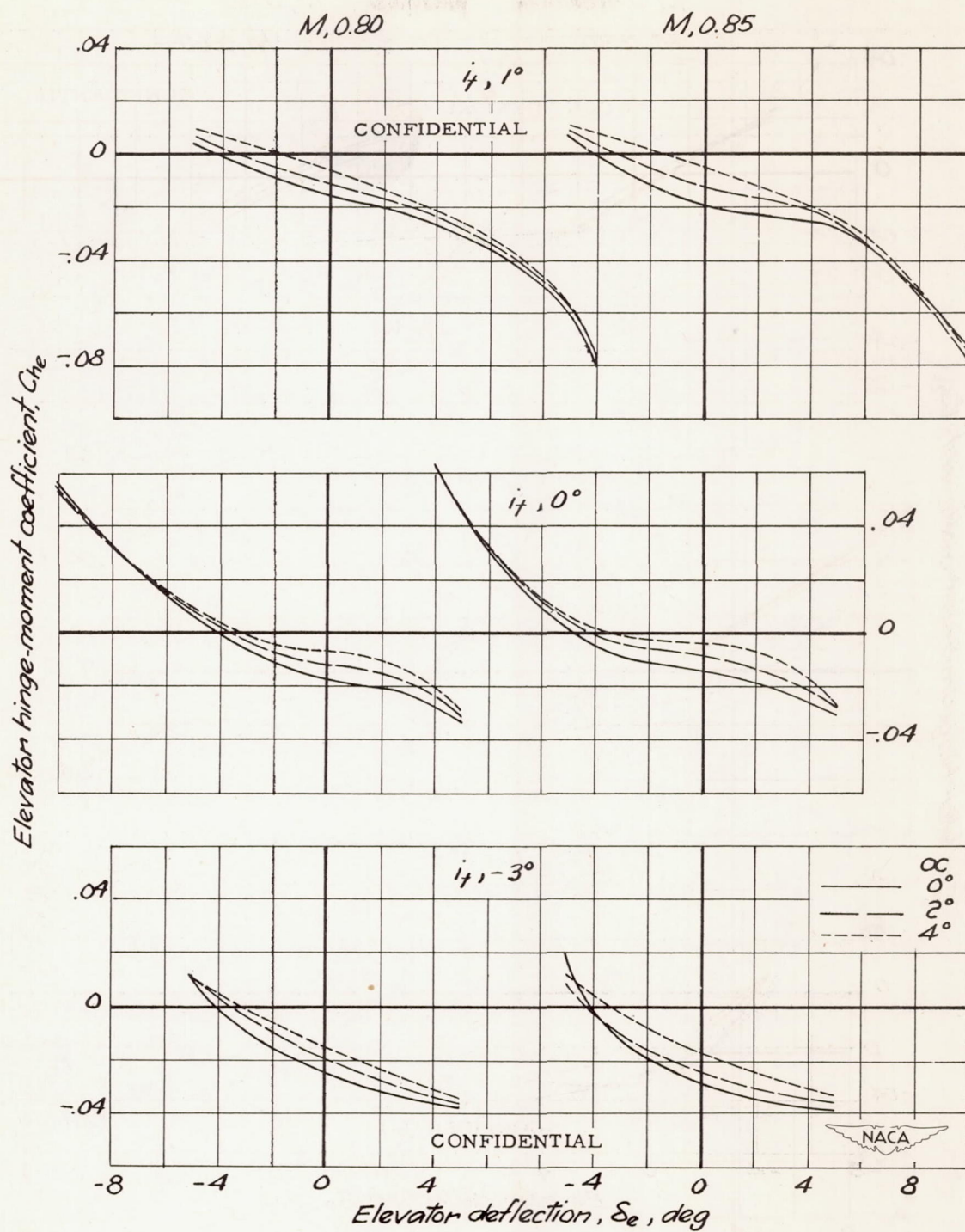
Figure 10.- Elevator effectiveness with zero stabilizer incidence and stabilizer effectiveness with zero elevator deflection ; C_L , 0
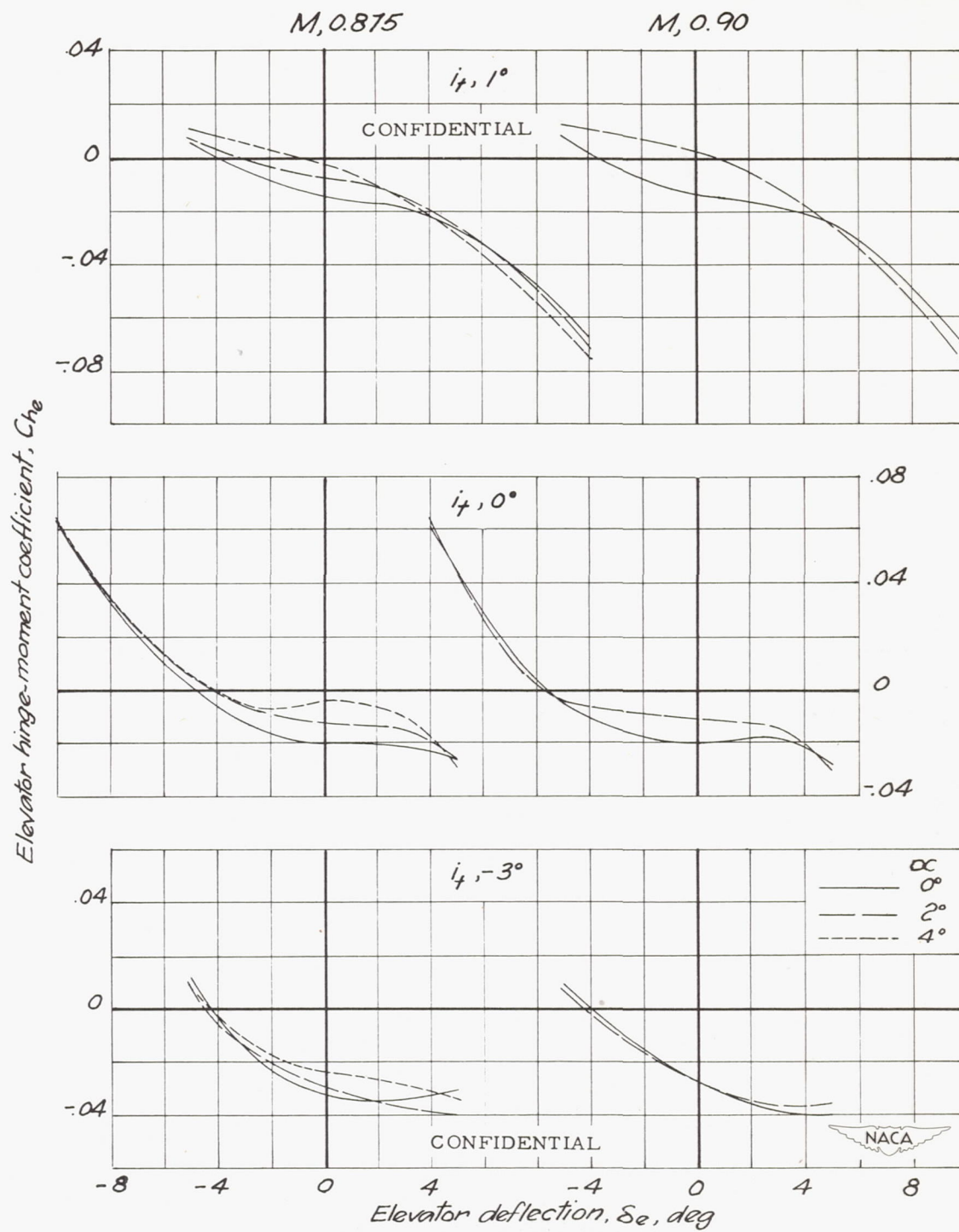
(a) M, 0.30, 0.60

Figure 11.- Elevator hinge-moment characteristics
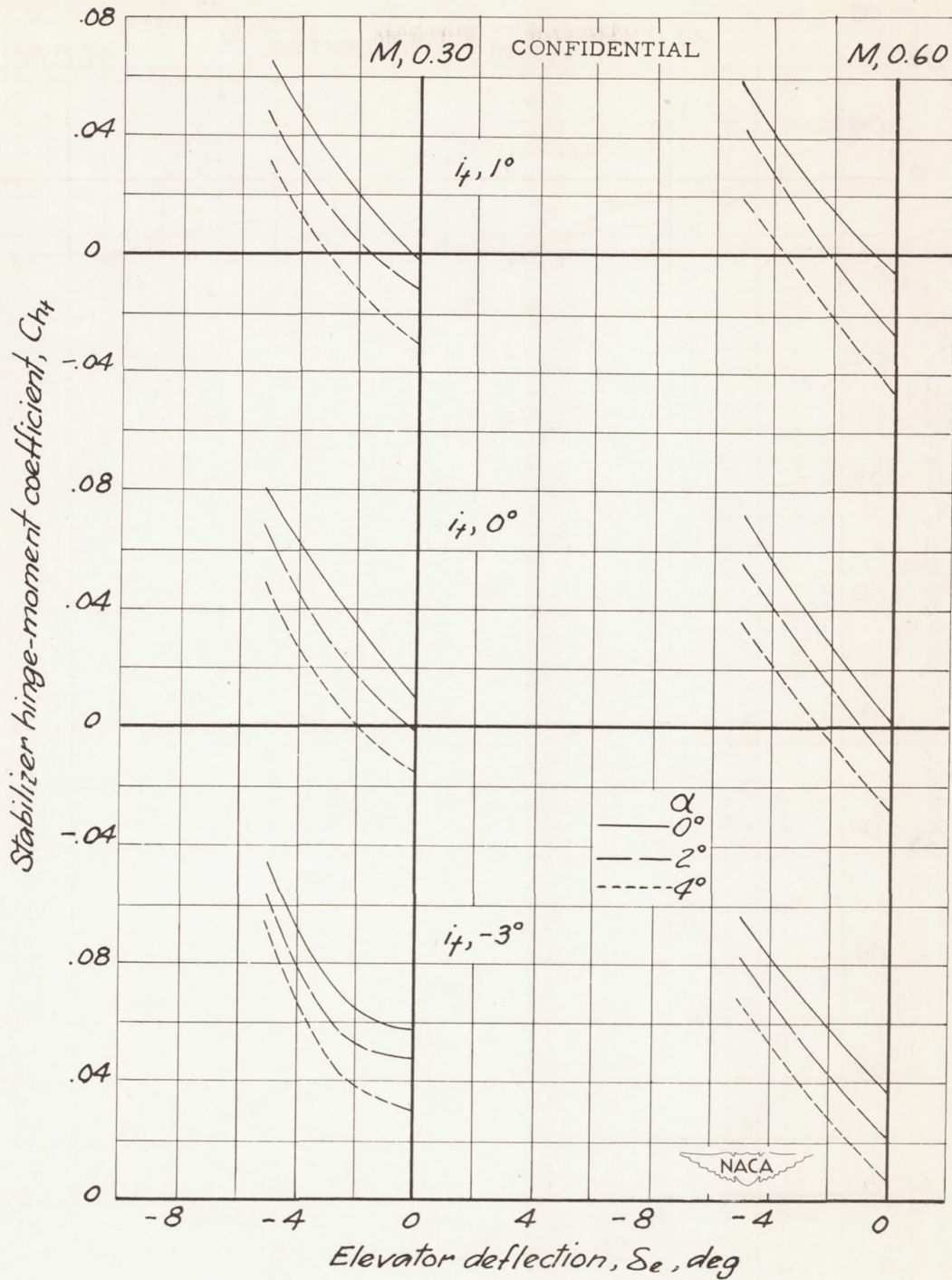
(b) M, 0.80, 0.85

Figure 11.-(Continued)

M, 0.875   M, 0.90

$i_t, 1°$

CONFIDENTIAL

$i_t, 0°$

$i_t, -3°$

α
0°
2°
4°

CONFIDENTIAL

NACA

Elevator hinge-moment coefficient, C_{h_e}

Elevator deflection, δ_e, deg
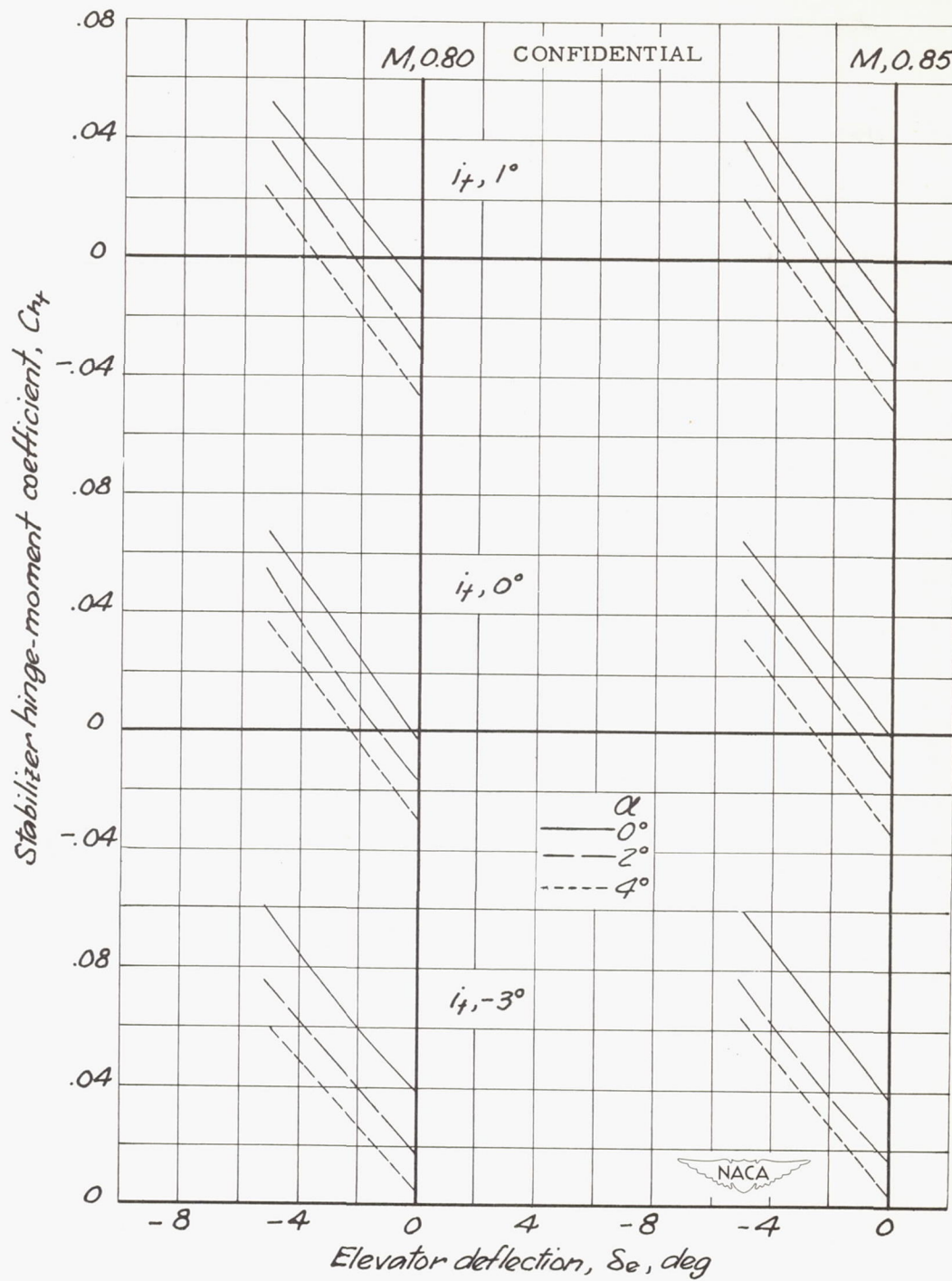
(c) M, 0.875, 0.90

Figure 11. – (Concluded)
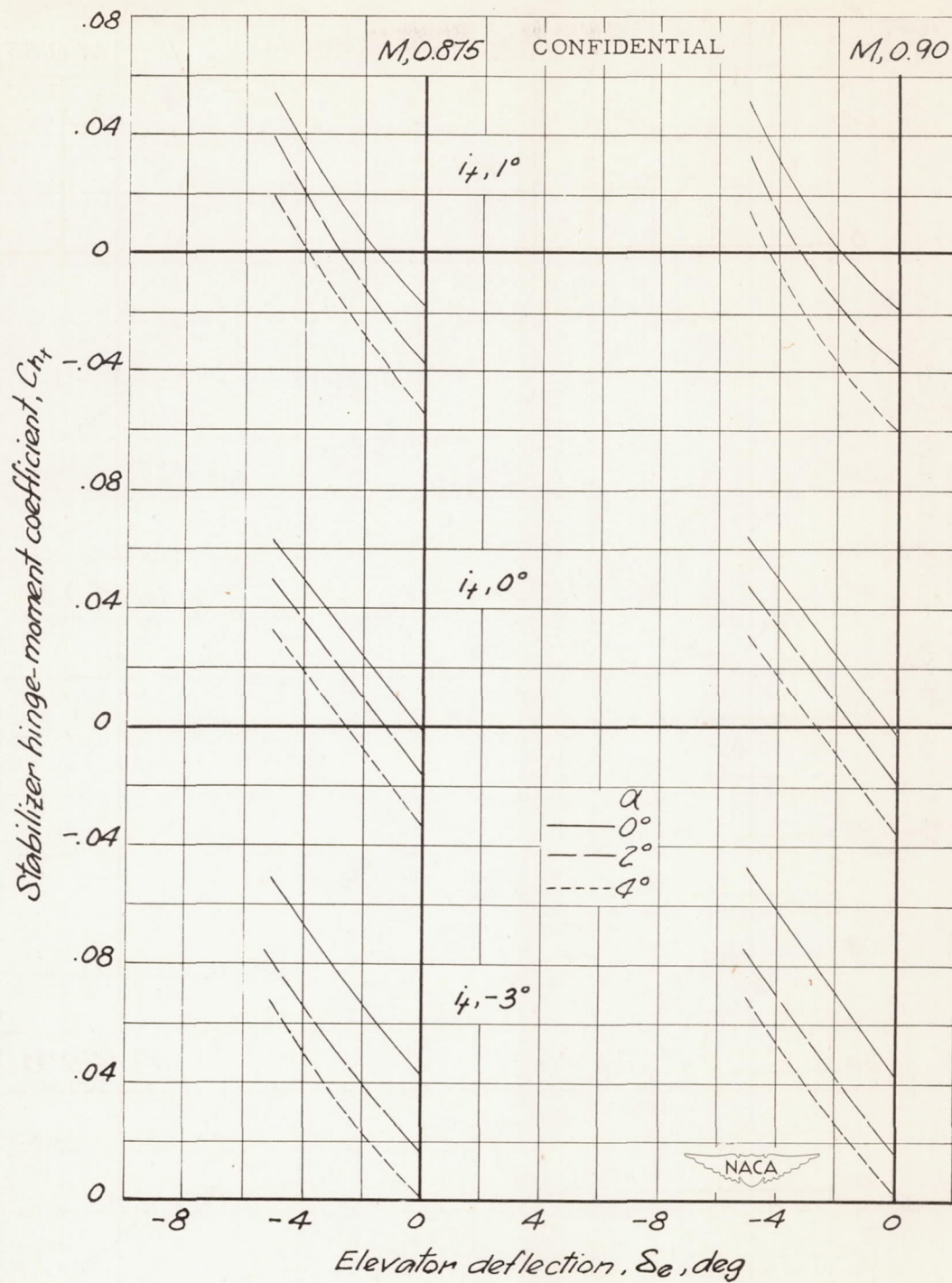
(a) M, 0.30, 0.60

Figure 12.- Variation of stabilizer hinge-moment
coefficient with elevator deflection

(b) M, 0.80, 0.85

Figure 12.- (Continued)

(c) M, 0.875, 0.90

Figure 12. - (Concluded)
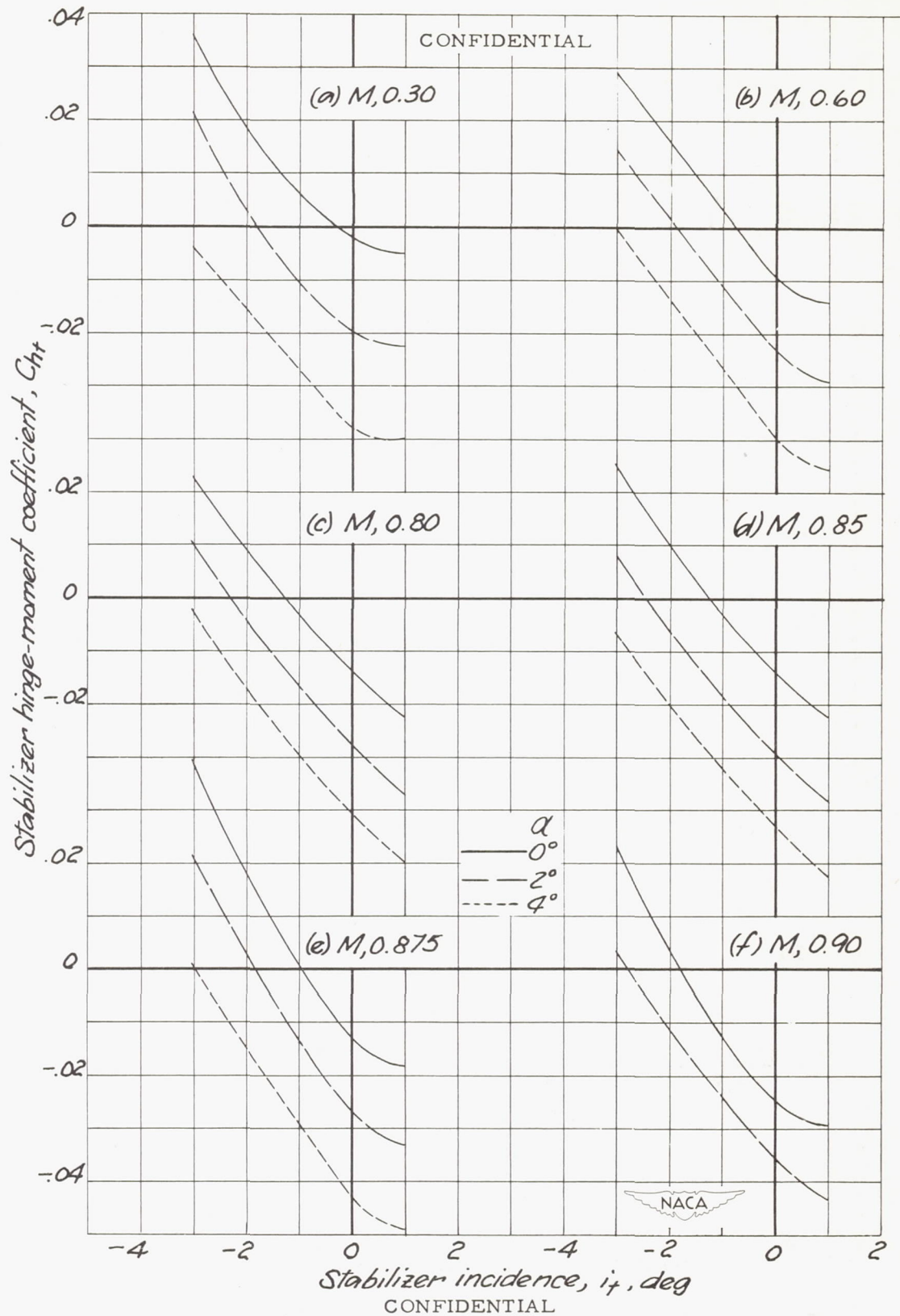
Figure 13.- Stabilizer hinge-moment characteristics
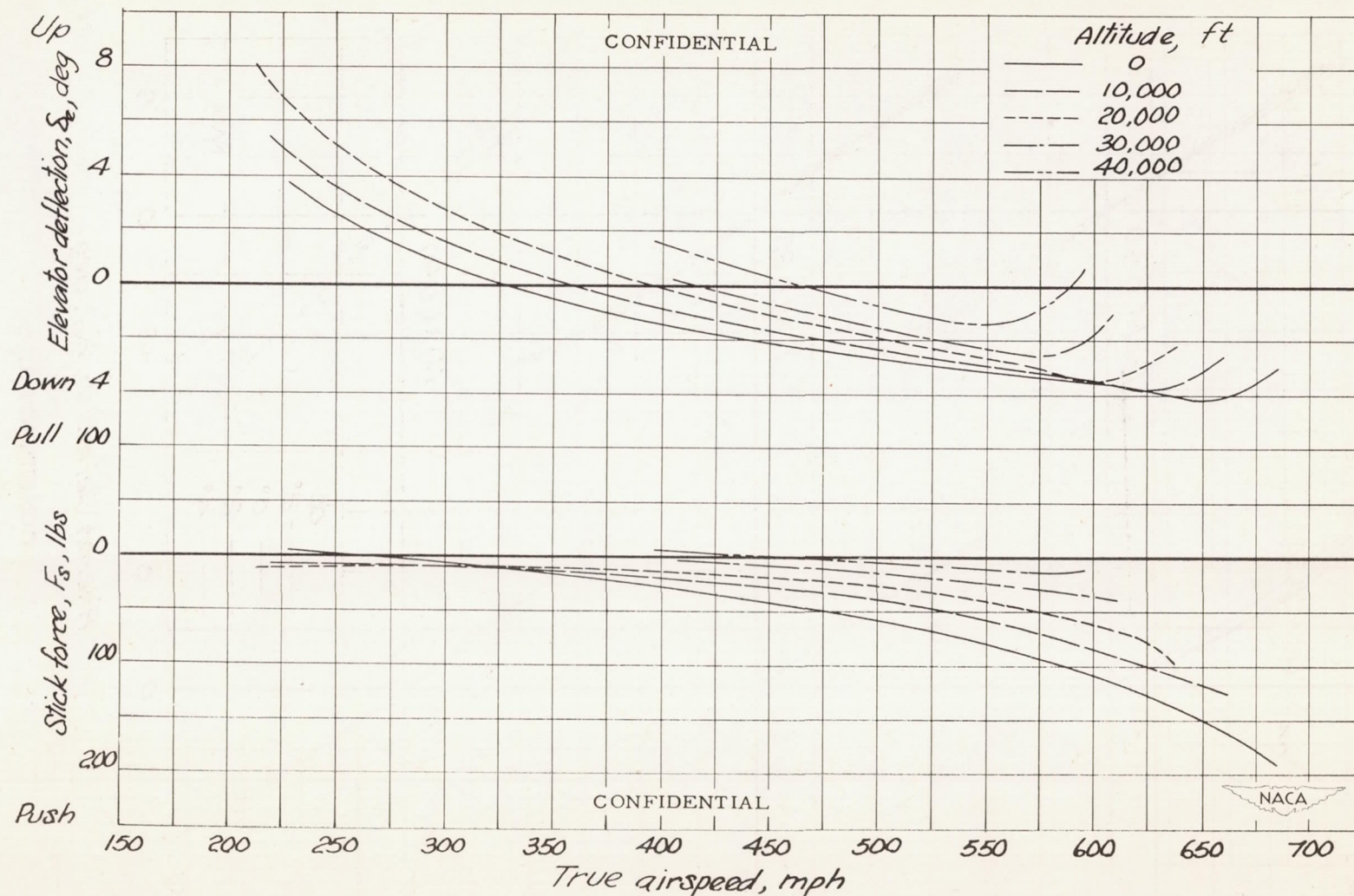
Figure 14.- Variation with airspeed of elevator deflection and stick force for level flight
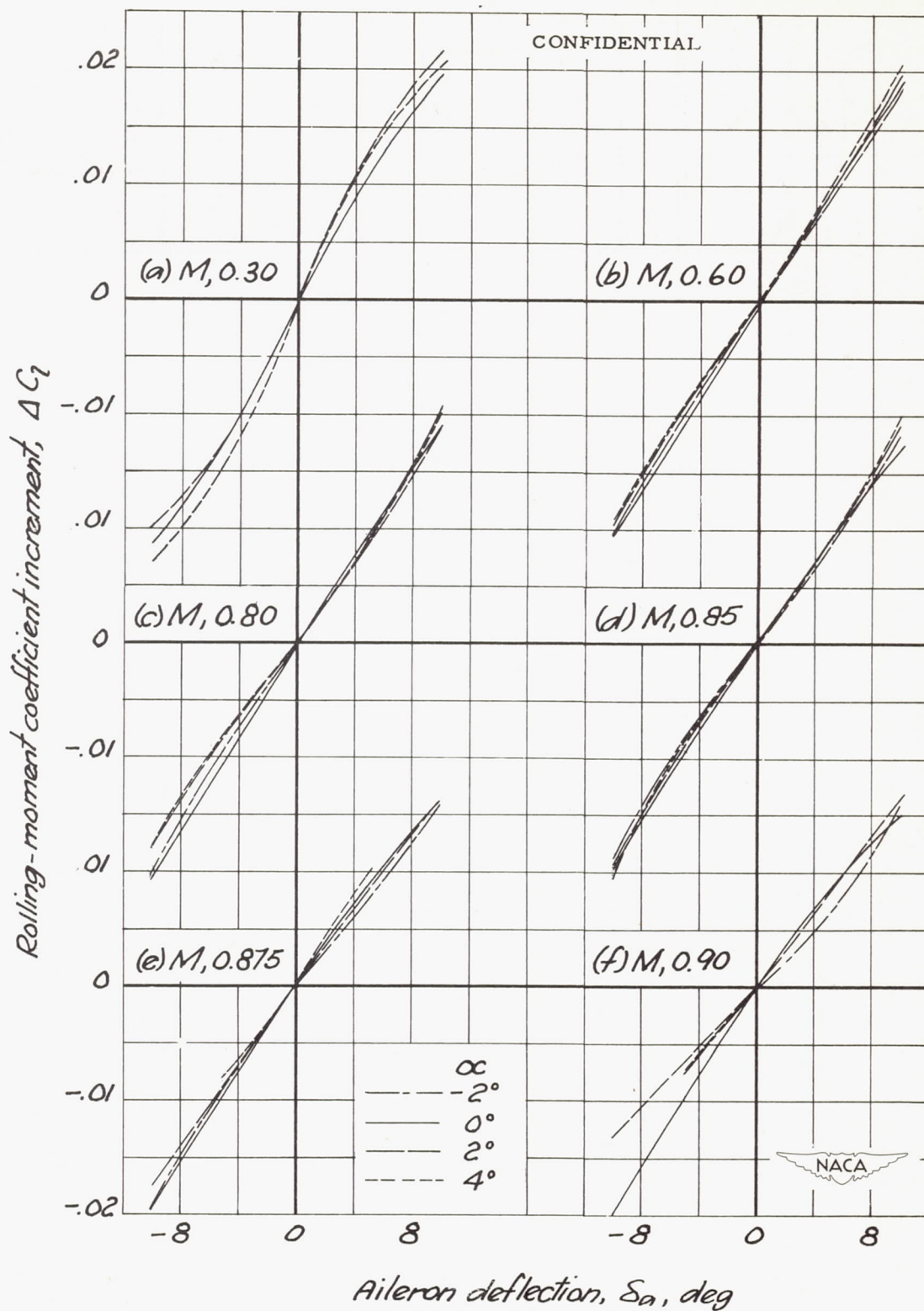
CONFIDENTIAL

Figure 15.— Aileron effectiveness
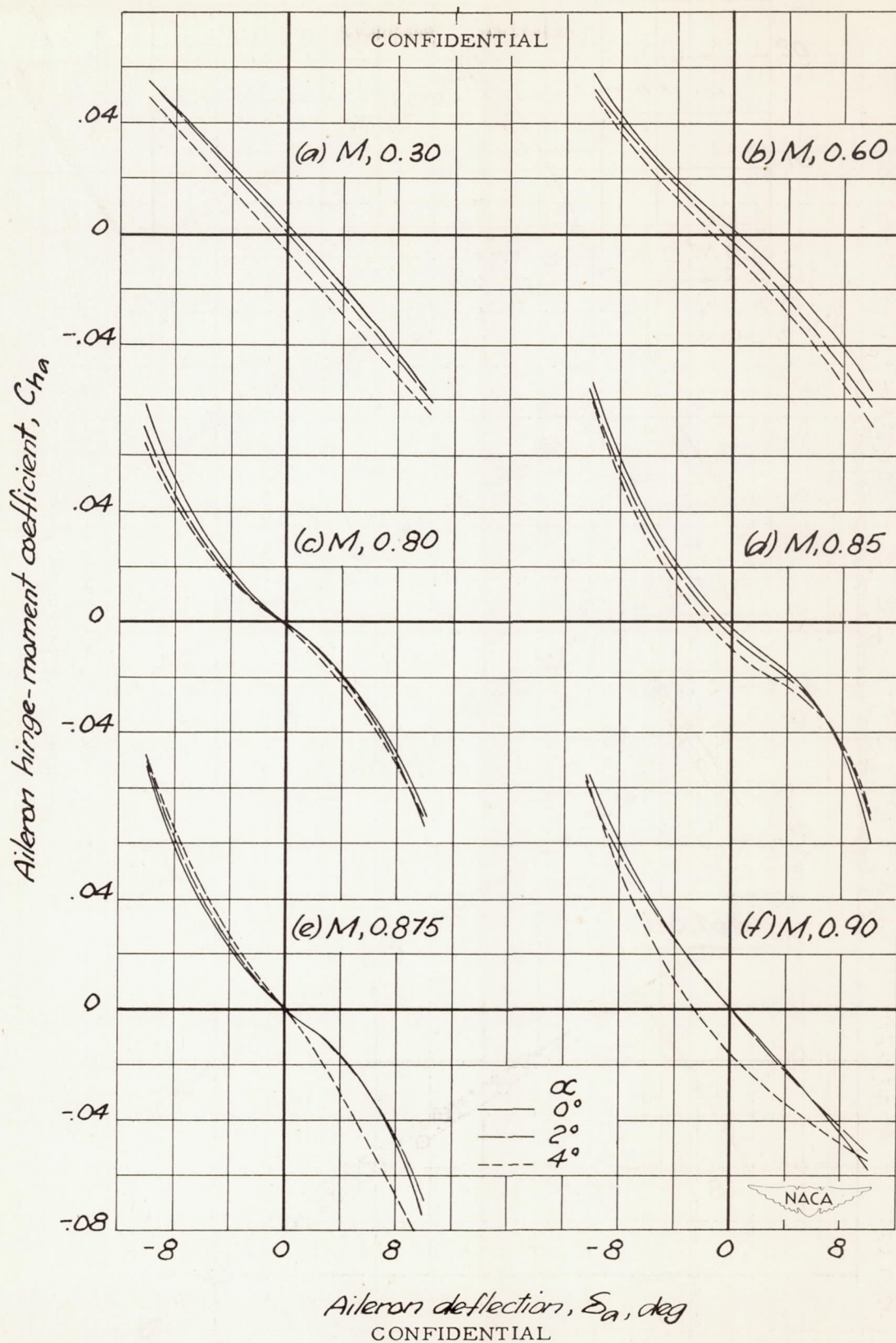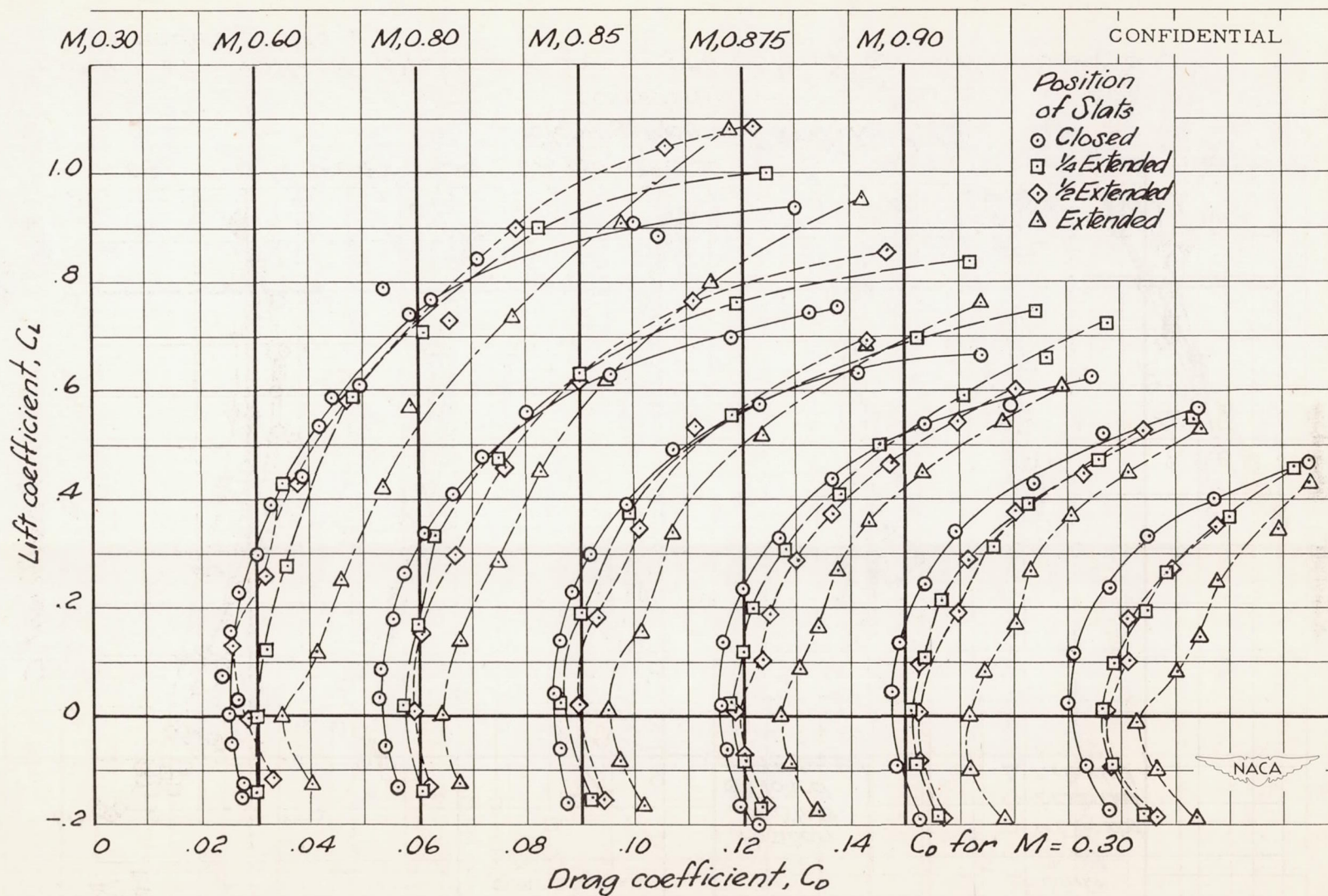
CONFIDENTIAL

Figure 16.- Aileron hinge-moment characteristics

Figure 17.— Lift characteristics with closed and extended slats

M, 0.30   M, 0.60   M, 0.80   M, 0.85   M, 0.875   M, 0.90

Position
of Slats
⊙ Closed
◻ ¼ Extended
◇ ½ Extended
△ Extended

Lift coefficient, C_L

1.0

.8

.6

.4

.2

0

-.2

0   .02   .04   .06   .08   .10   .12   .14 C_D for M = 0.30

Drag coefficient, C_D

Figure 18.- Drag characteristics with closed and extended slats
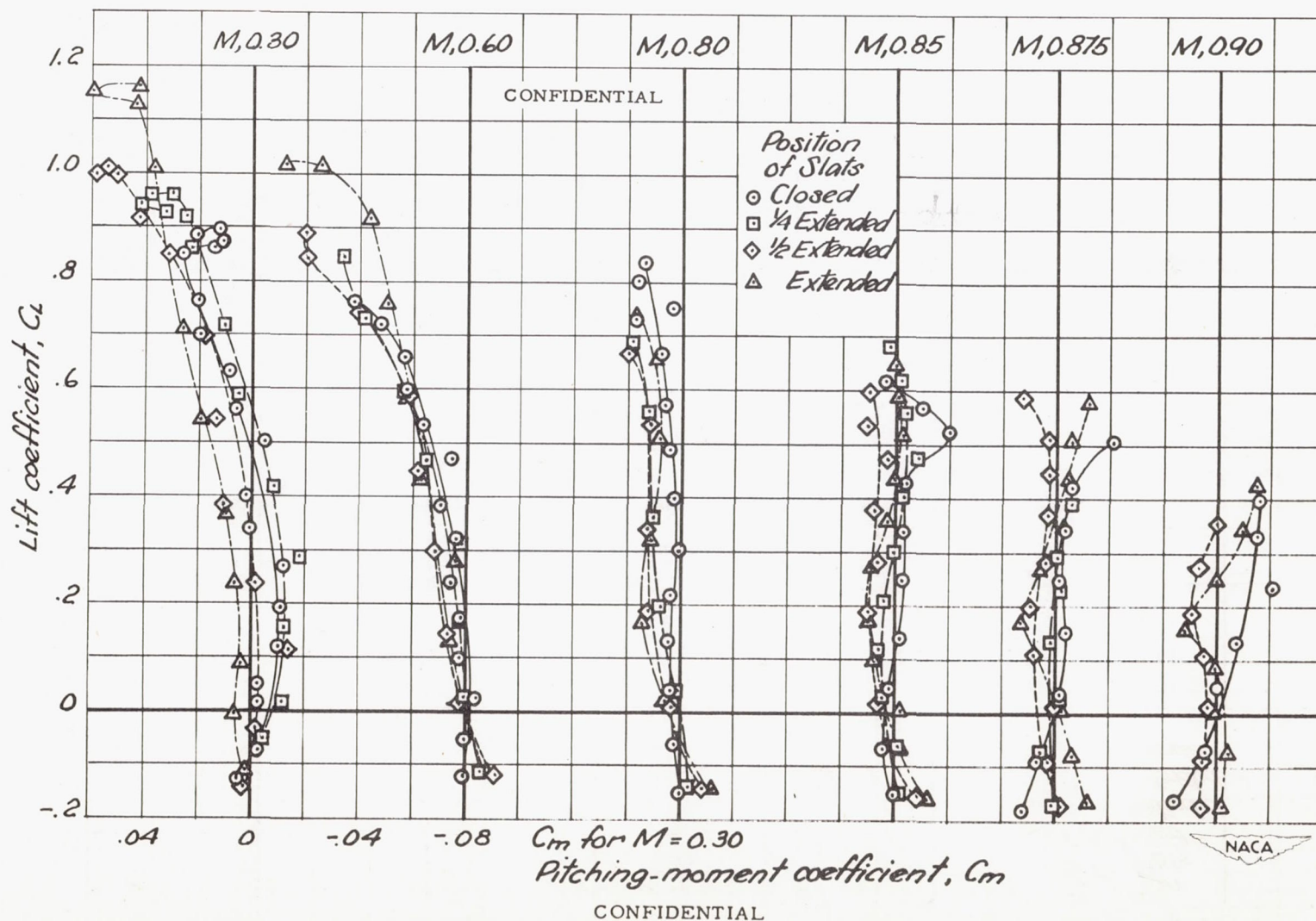
Figure 19.- Tail-off pitching-moment characteristics with closed and extended slats
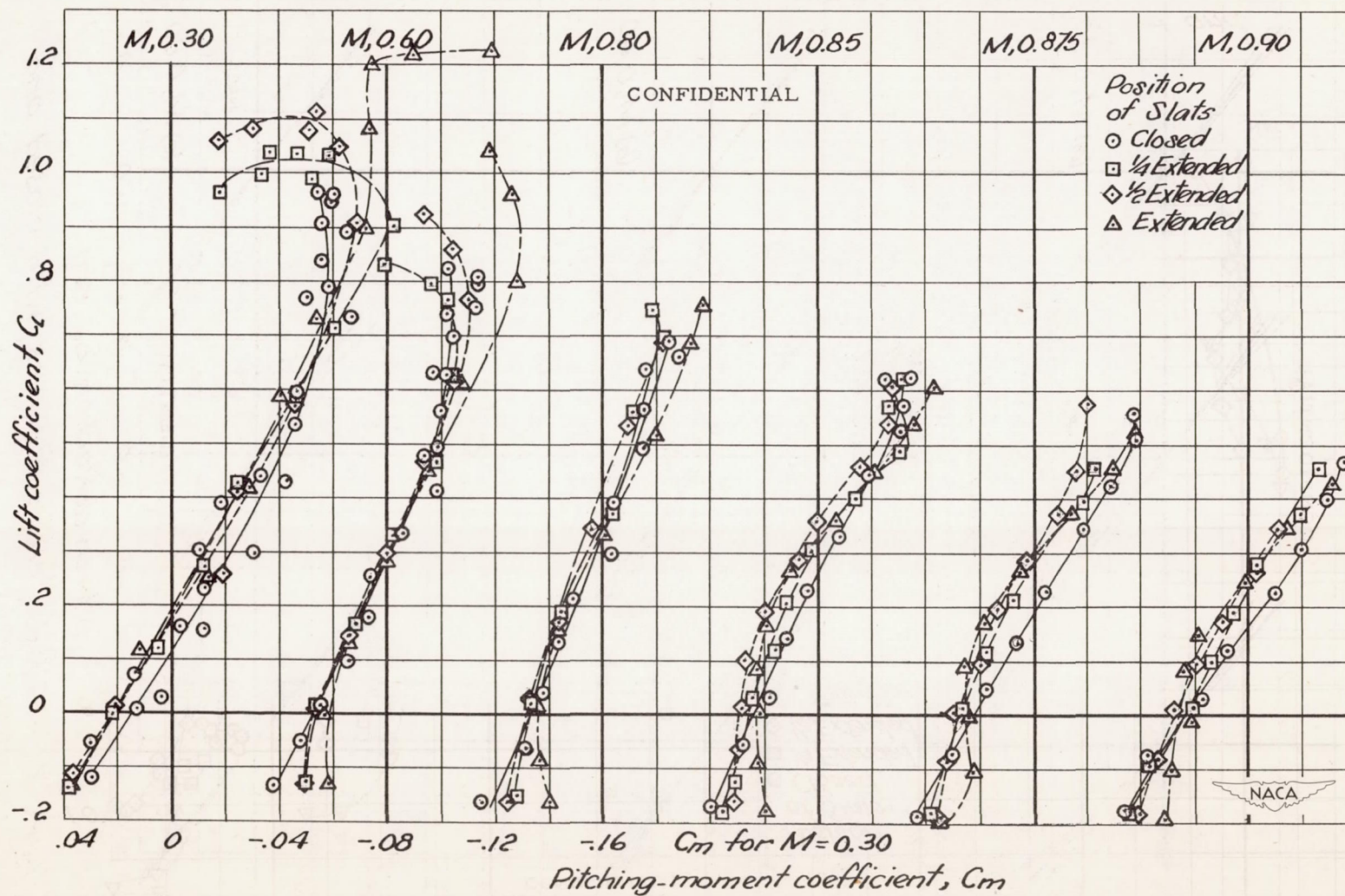
Figure 20.— Tail-on pitching-moment characteristics with closed and extended slats
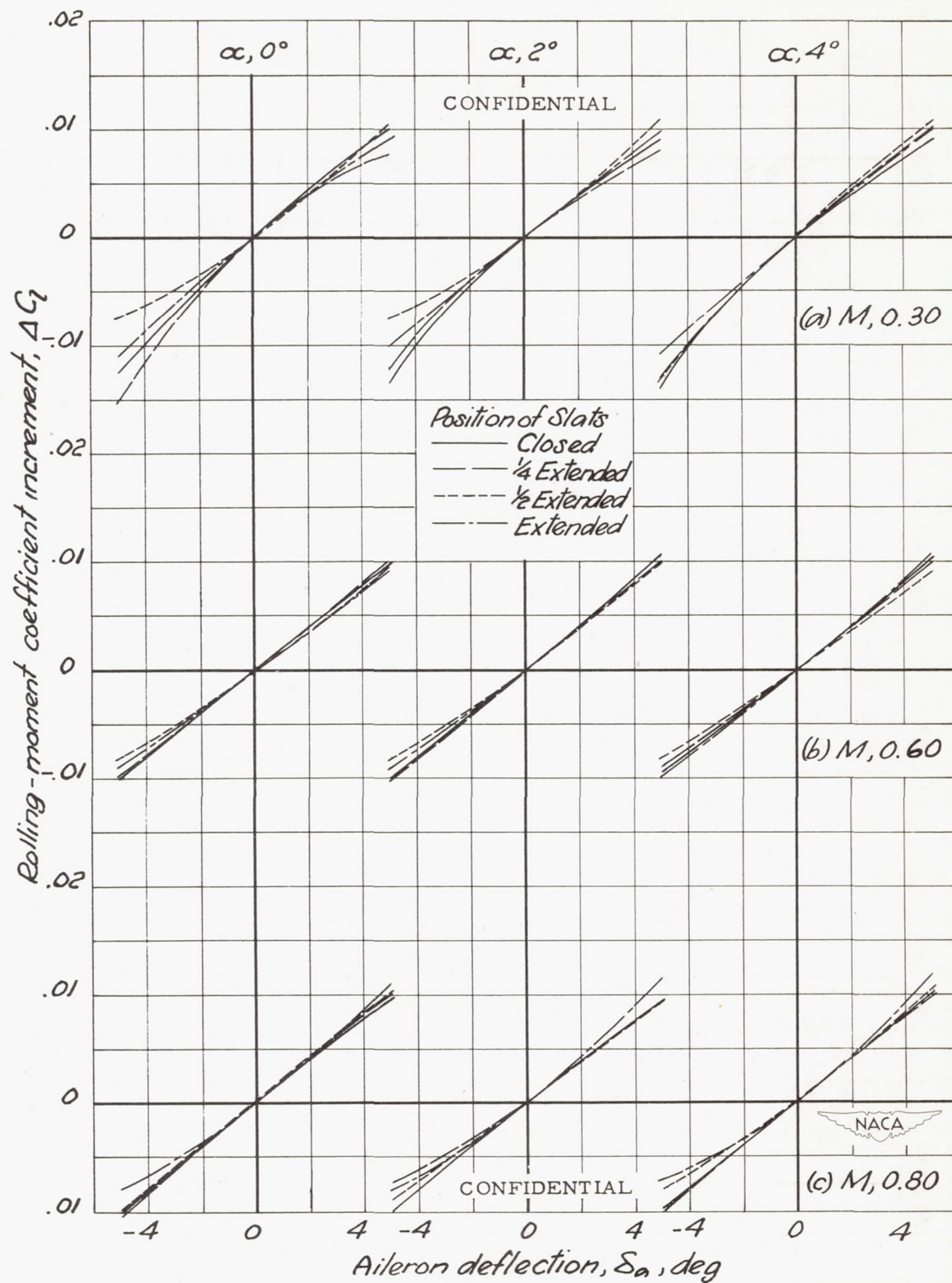
Figure 21.– Aileron characteristics with closed and
   extended slats

Figure 21.- (concluded)

CONFIDENTIAL

δ_B
⊙ 0°
□ 20°
◇ 40°
△ 85°

α for M = 0.30

Angle of attack, α, deg

CONFIDENTIAL

Lift coefficient, C_L

M, 0.30   M, 0.60   M, 0.80   M, 0.85   M, 0.875   M, 0.90
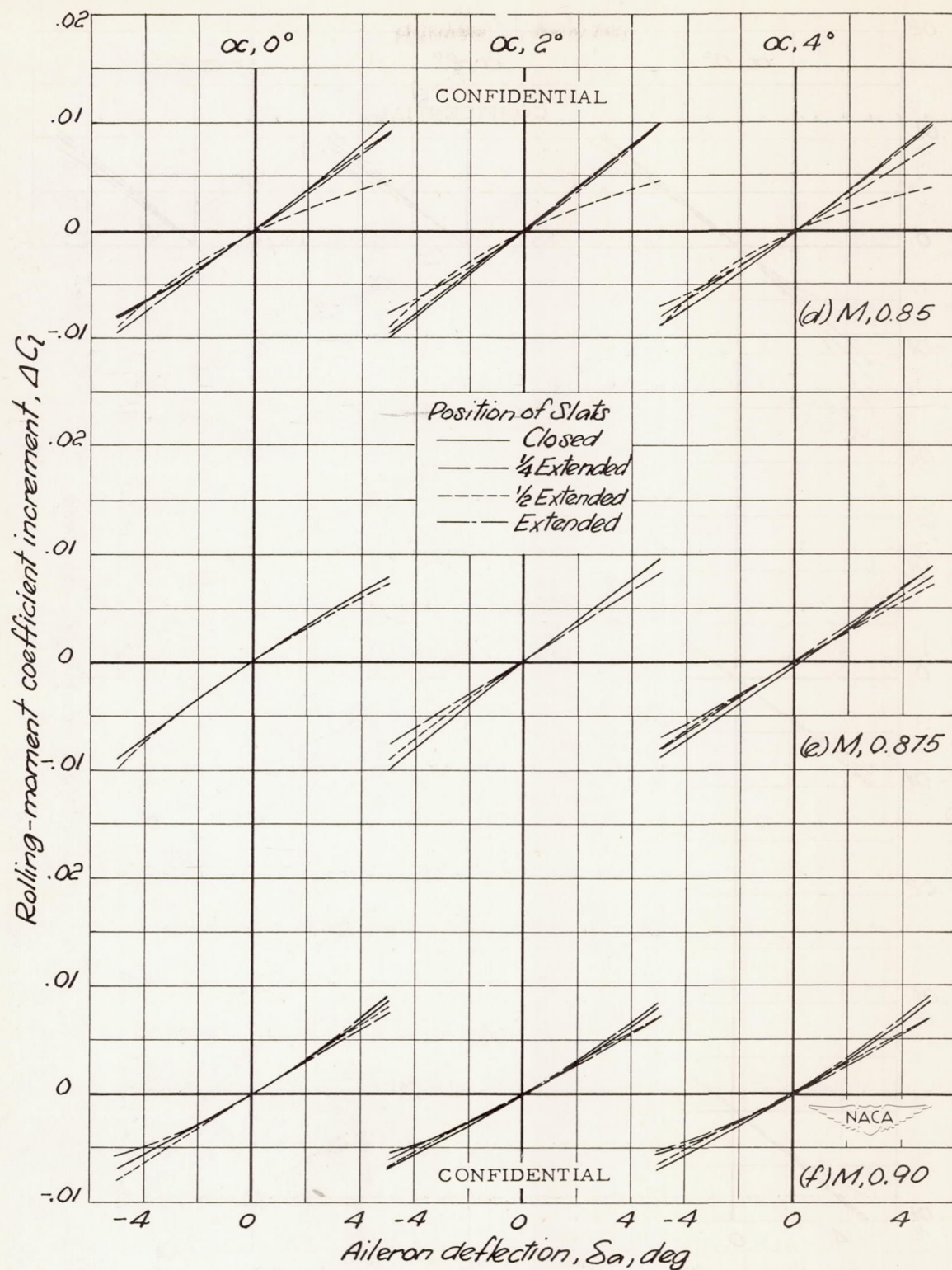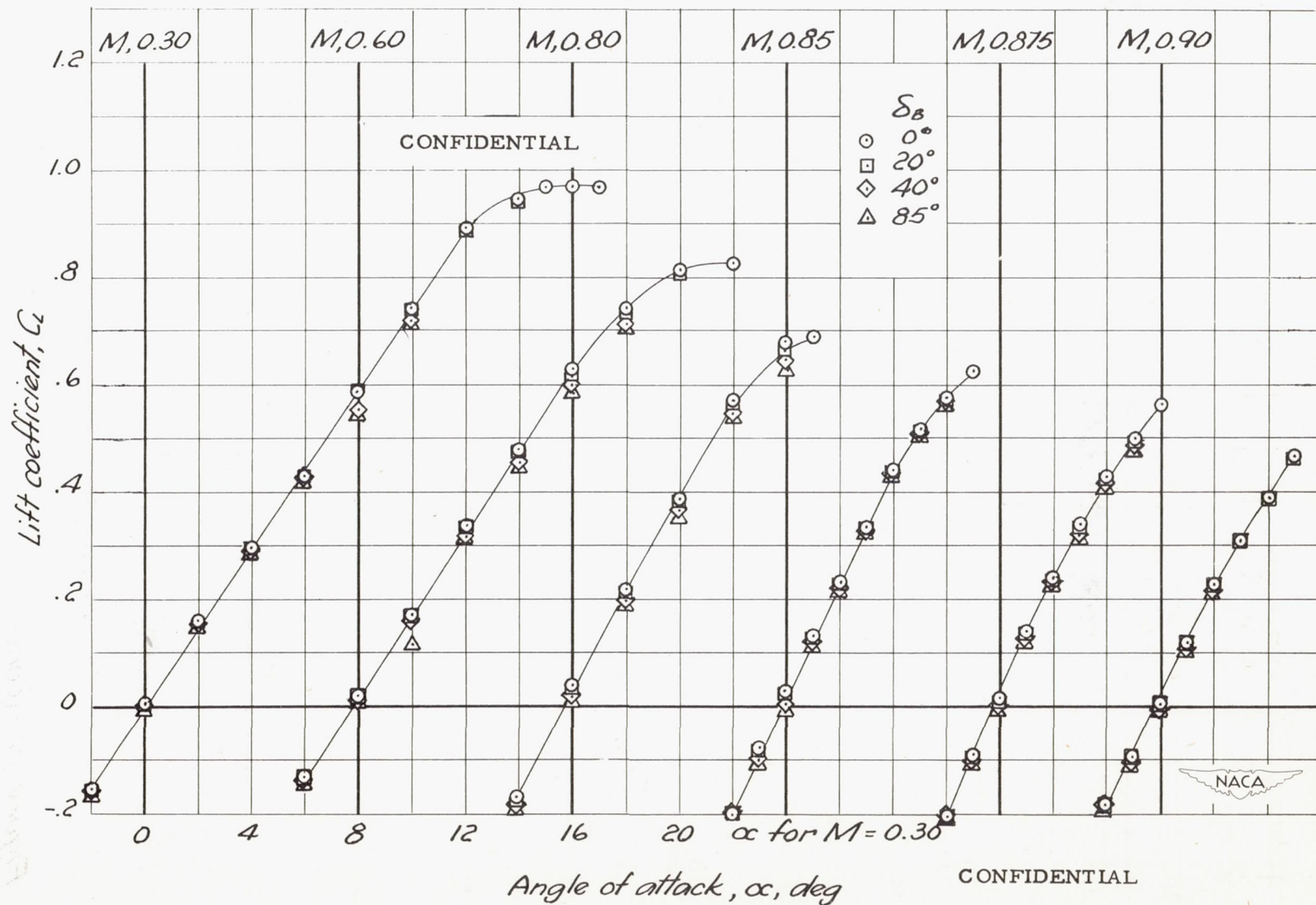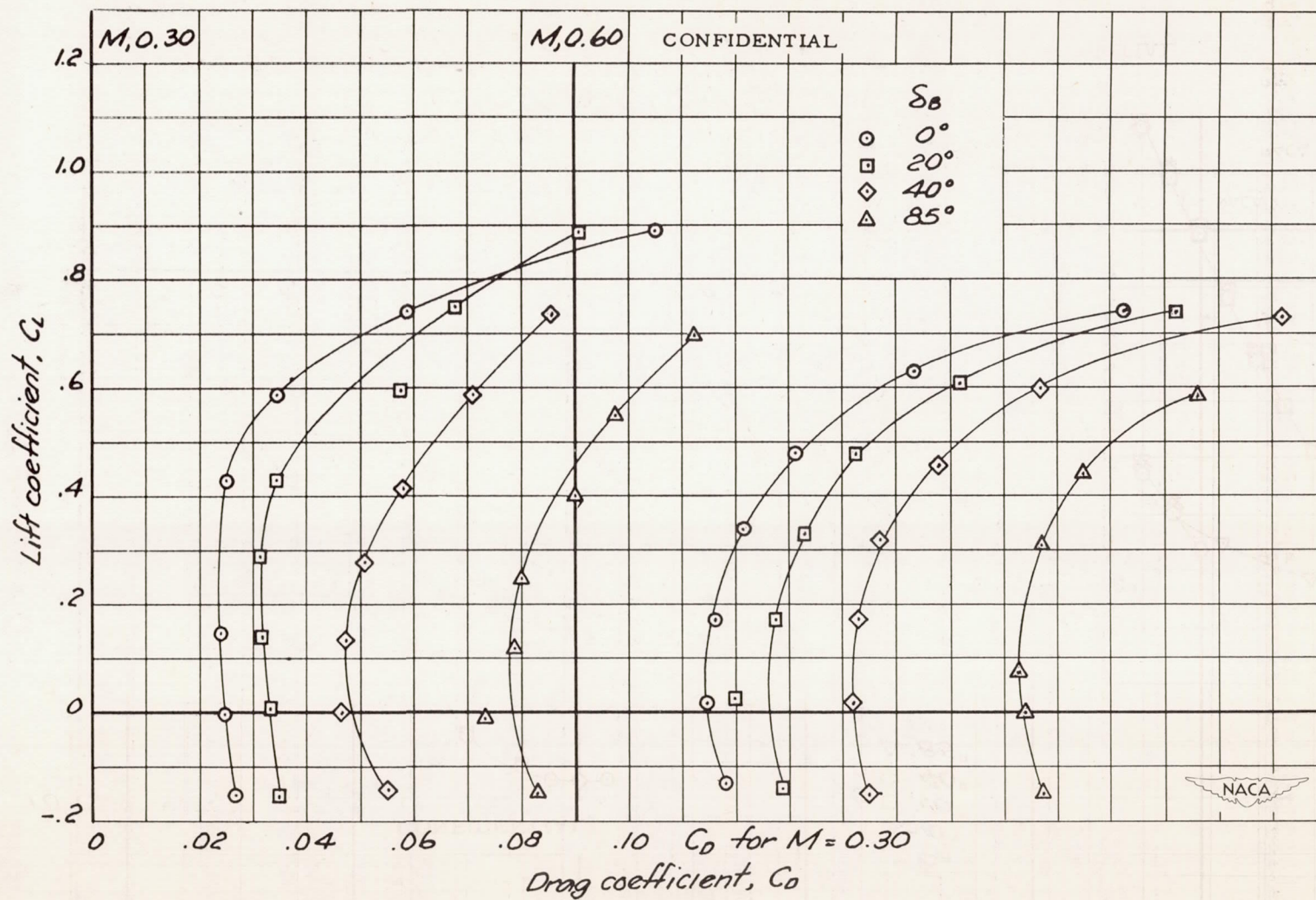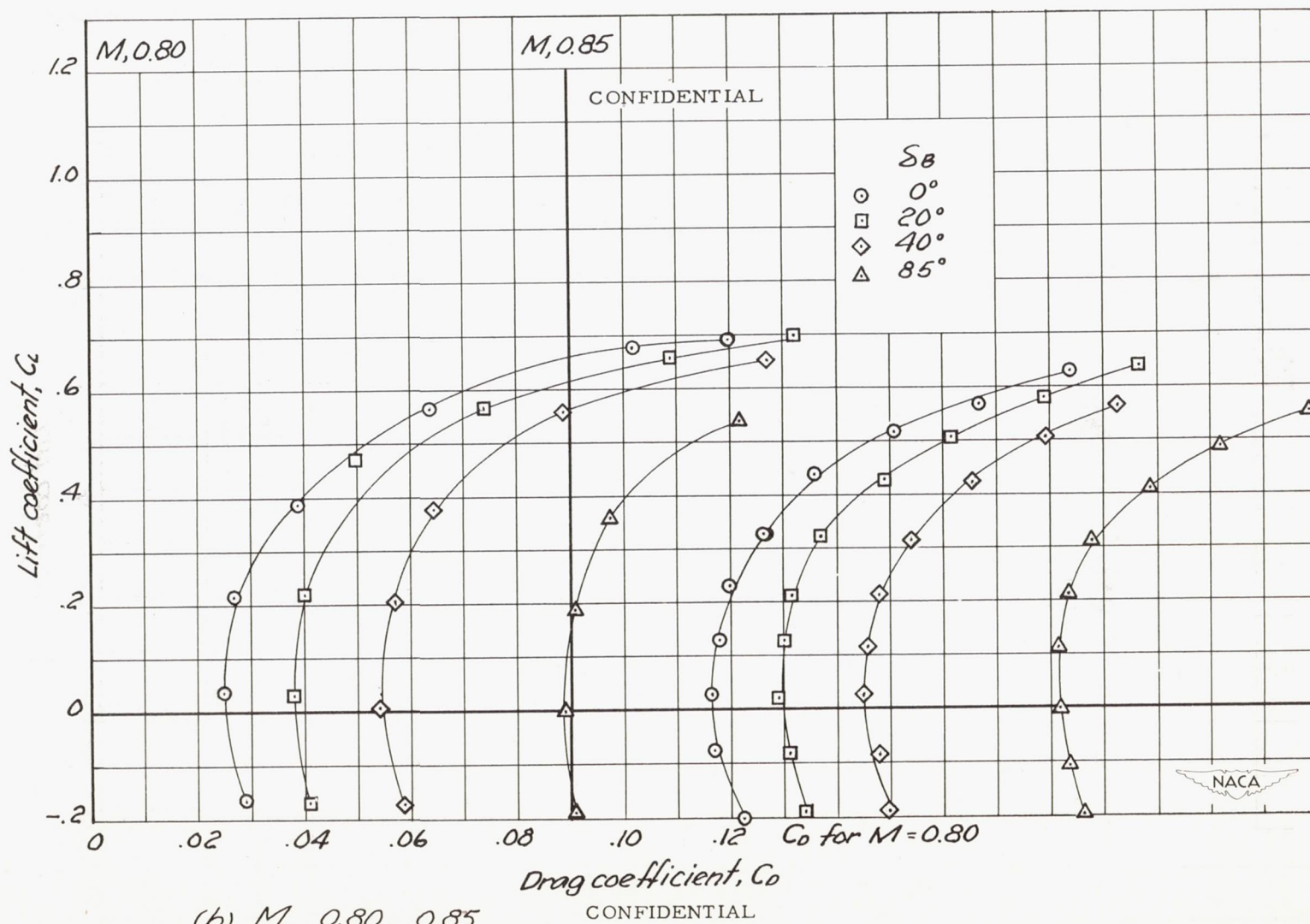
Figure 22.- Lift characteristics with dive brake closed and deflected

(a) M, 0.30, 0.60
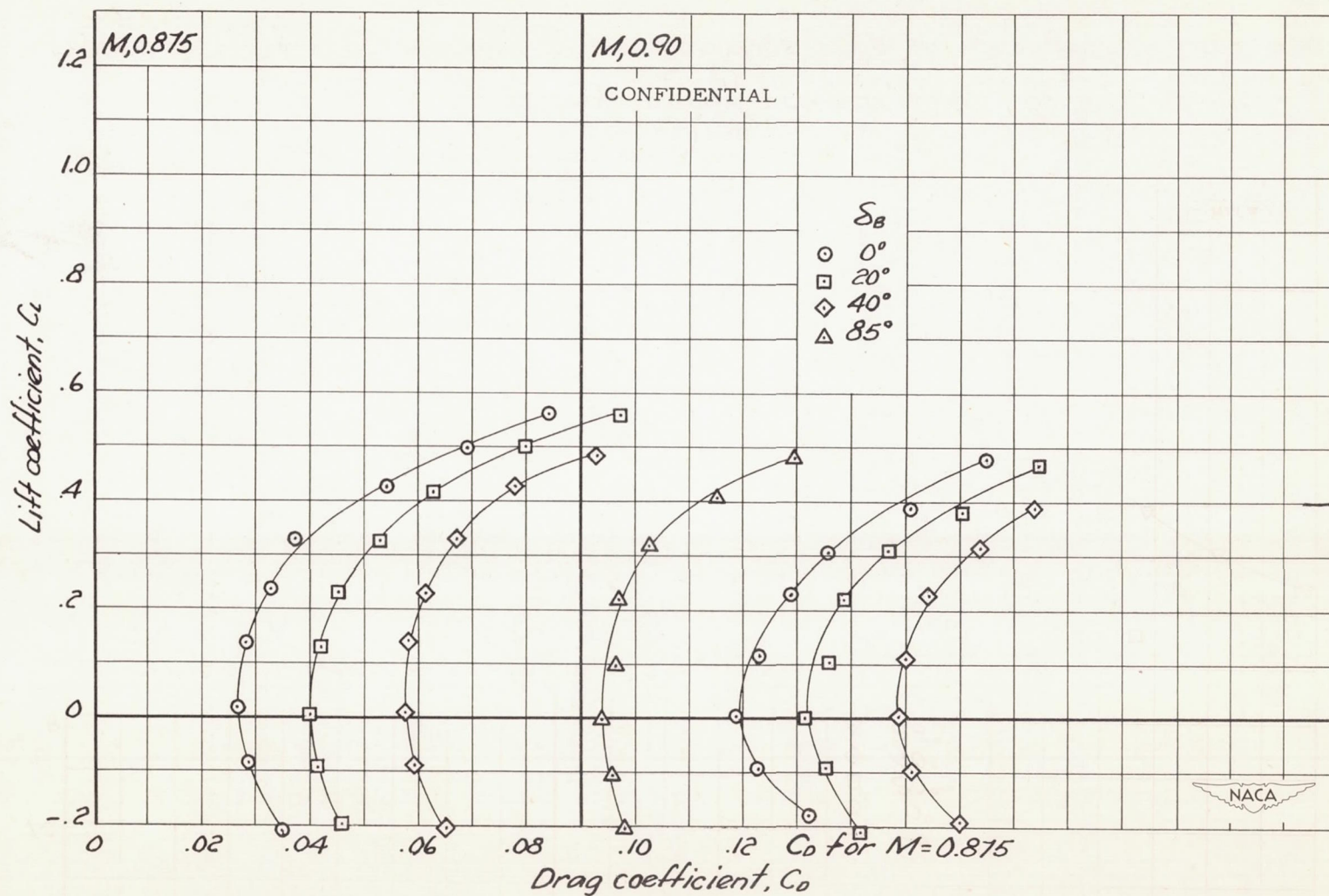
CONFIDENTIAL

Figure 23.-Drag characteristics with the dive brake closed and deflected

(b) M, 0.80, 0.85

Figure 23.- (Continued)

CONFIDENTIAL

δ_B
⊙ 0°
⊡ 20°
◇ 40°
△ 85°

Co for M=0.875

(c) M, 0.875, 0.90

Figure 23.- (Concluded)
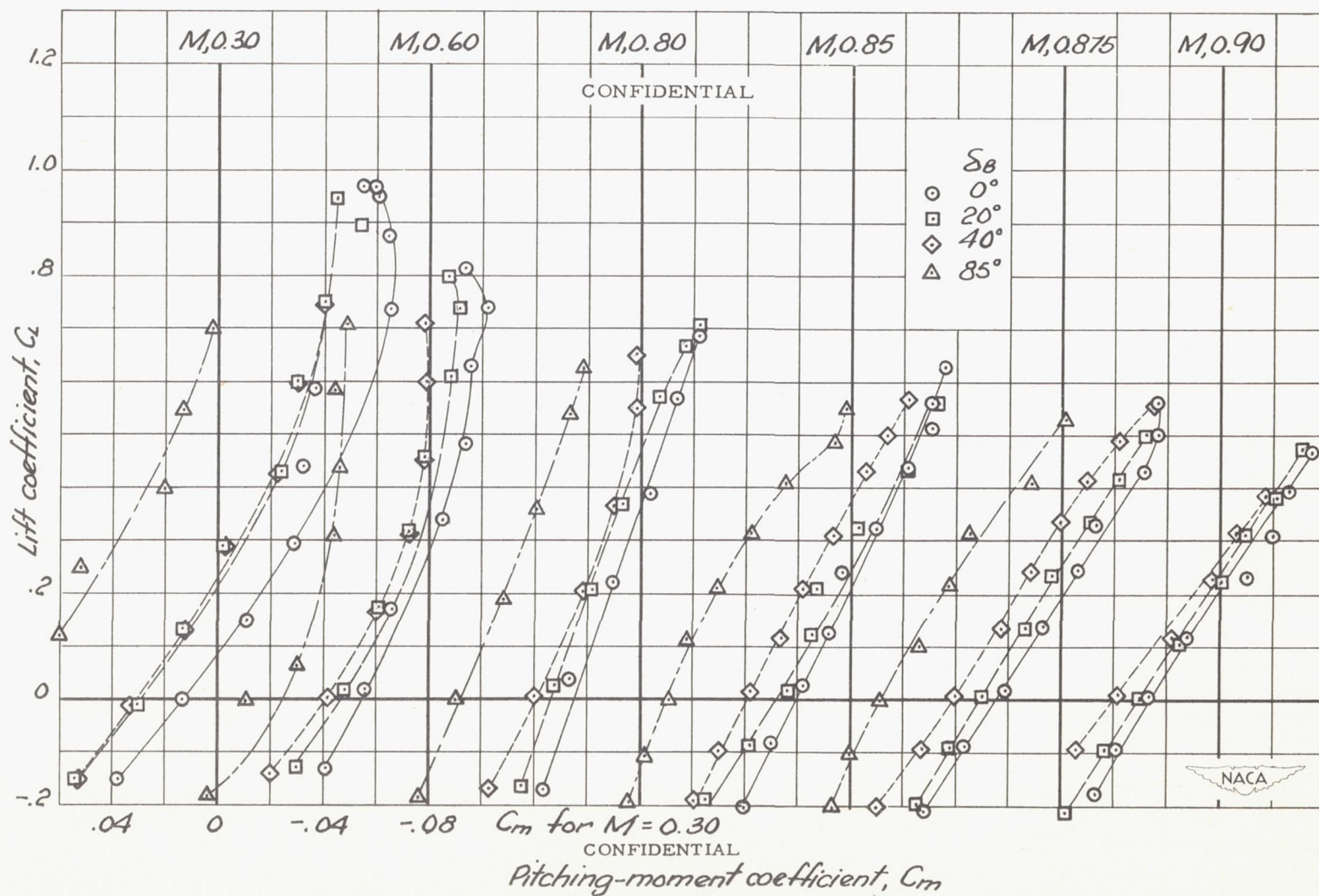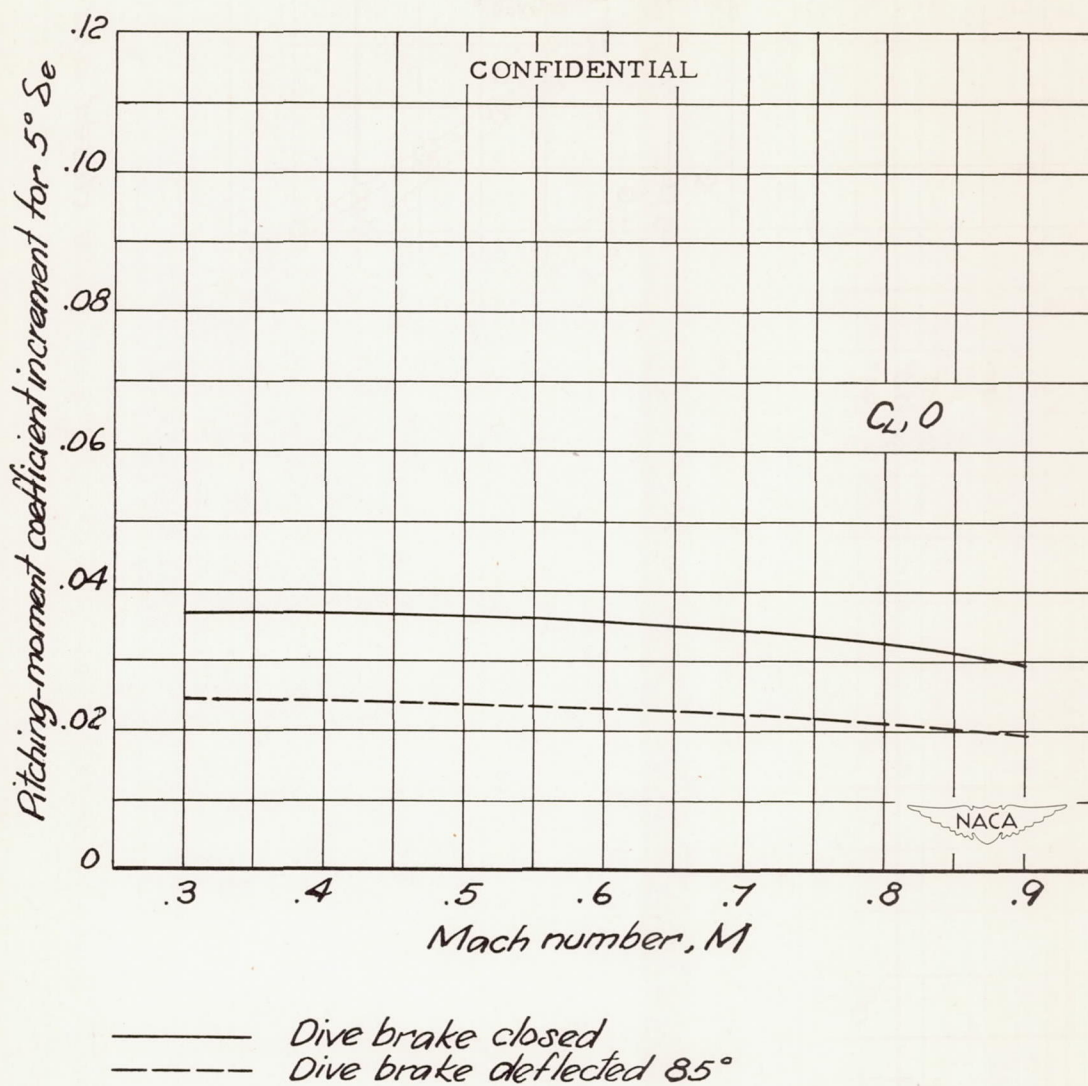
CONFIDENTIAL

Figure 24.— Pitching-moment characteristics with the dive brake closed and deflected

Figure 25.- Elevator effectiveness with dive brake closed and deflected